Gastruloids employ an alternative morphogenetic route to generate a posterior body axis on adherent substrates

Guillermo Serrano Nájera[1*†], Apolline Delahaye[1†], and Benjamin J. Steventon[1*]

[1]Department of Genetics, University of Cambridge, Cambridge, CB2 3EH, UK
[*]Emails for correspondence: guillermo.serrano-najera@gen.cam.ac.uk, bjs57@cam.ac.uk
[†]Equal contribution

Morphogenesis emerges from the integration of genetic programs with environmental signals, yet studying this interplay in embryos remains challenging due to the inherent complexity of embryonic systems, with their multiple interacting tissues and maternal influences. Using gastruloids as an accessible model, we systematically investigated how extracellular matrix composition directs morphogenetic strategies. We discovered that gastruloid substrate adhesion profiles evolve with differentiation state: while early aggregates attach only to laminin, mesoderm specification enables adhesion to fibronectin and collagens, possibly recapitulating sequential ECM deposition during embryogenesis. On laminin, gastruloids form flat structures with multiple radiating cell streams that maintain proper anterior-posterior gene expression patterns, demonstrating that gastruloids can elongate a patterned body axis using substrate-cell interactions instead of the cell-cell interactions seen in free-floating counterparts. Testing this through pharmacological inhibition of cytoskeletal components revealed unexpected substrate-specific requirements: blocking lamellipodia paradoxically enhanced cell-stream elongation, while blocking filopodia prevented its formation entirely. Crucially, these same inhibitors have no effect on free-floating gastruloids, demonstrating that tissues possess multiple, context-dependent routes to achieve axis elongation. Our findings establish that developing tissues harbour latent morphogenetic plasticity, and the ability to deploy alternative cellular mechanisms based on environmental context while preserving core developmental programs. This flexibility may provide insights into how evolution might explore morphological diversity without disrupting essential patterning, and suggests new strategies for controlling form in tissue engineering.

Keywords— Gastruloids, ECM, Developmental plasticity, Morphogenesis, Lamellipodia, Filopodia

Introduction

Morphogenesis emerges from the dynamic integration of genetic programs with environmental signals, where physical and chemical cues actively instruct developmental outcomes. External boundary conditions such as geometry, mechanical properties, and chemical composition of the medium are fundamental determinants of morphogenetic strategies, yet studying these interactions in developing embryos remains challenging due to maternal constraints, system complexity, and limited experimental accessibility.

Gastruloids are three-dimensional aggregates of embryonic stem cells stripped of the extrinsic signals present in the embryo. Remarkably, gastruloids spontaneously recapitulate key aspects of vertebrate gastrulation, including germ layer formation, and coordinated morphogenetic movements that establish a patterned body axis (Van den Brink et al., 2014; Van Den Brink et al., 2020) characterised by the expression of retinoic acid in the anterior tissues and WNT and FGF towards posterior (del Corral and Storey, 2004; Martins-Costa et al., 2024; Anand et al., 2023). This system offers critical advantages including high experimental accessibility, reproducible conditions, and the ability to systematically manipulate environmental variables while preserving essential developmental programs (Steventon et al., 2021; van den Brink and van Oudenaarden, 2021). These features make gastruloids an ideal model system for investigating how external boundary conditions direct morphogenetic strategies during early development (Anlas and Trivedi, 2021; Morales et al., 2021; Serrano Nájera and Weijer, 2023).

During normal mammalian gastrulation, complex cell-substrate interactions drive key morphogenetic processes, including epithelial-to-mesenchymal transition (EMT) and cell migration through the primitive streak (Leptin, 2005). In amniotes, this process unfolds within a dynamically remodelling extracellular environment that begins with a laminin-rich basement membrane (Nakaya et al., 2008; Stower et al., 2015; Kyprianou et al., 2020) and progresses through sequential depo-

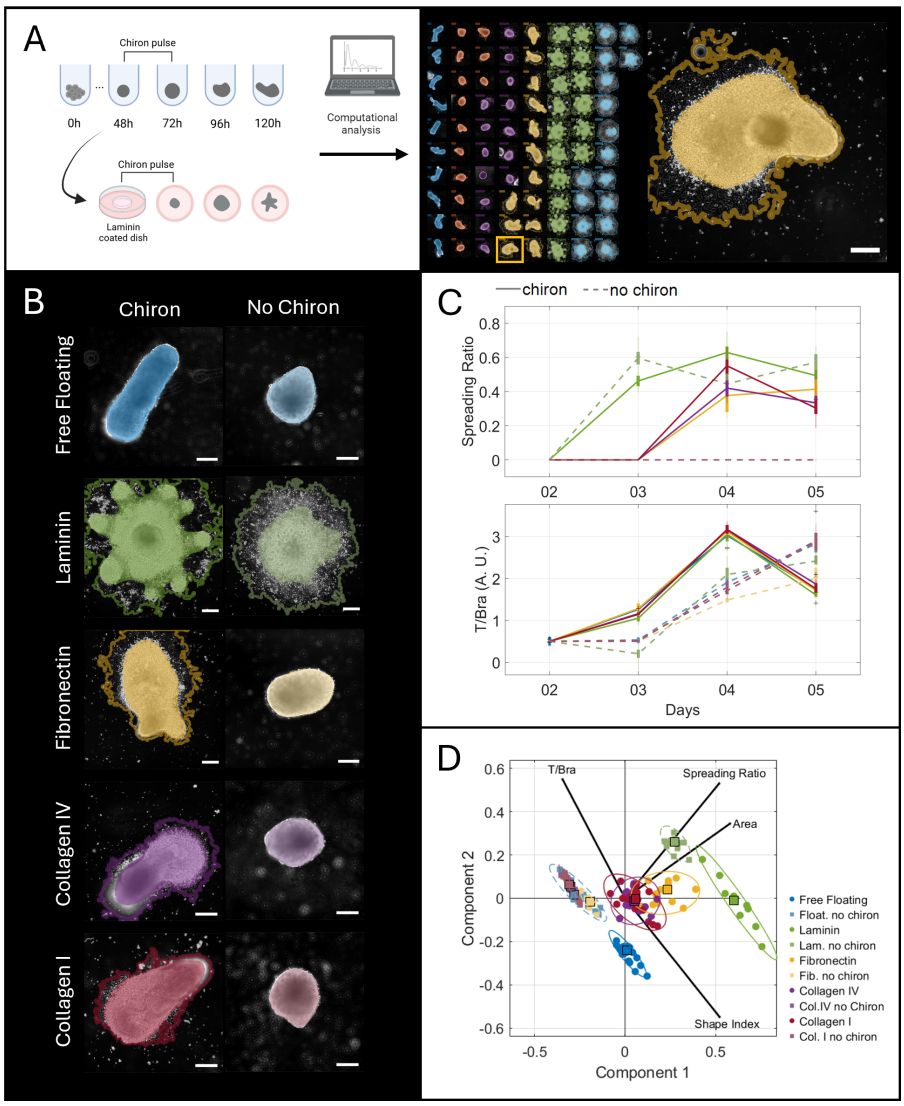

Fig. 1. Mesoderm specification regulates gastruloid substrate-adhesion profile. A) High-throughput production (left) and analysis (centre) of gastruloids on different substrates. In the close up (right) the continuous mask covers the main body of the gastruloid while the continuous line marks the limit of the migration front. B) Gastruloids exhibit diverse morphogenetic behaviours depending on the substrate and the presence of Chiron. C) Analysis of the spreading capability (spreading ratio) of gastruloids on different substrates (top) and T/Bra expression (bottom) from day 2 to 5. D) Principal Component Analysis integrating different properties on day 5 (see Fig. S1). Colours indicate the same conditions across graphs.

sition of collagens and fibronectin (Leivo et al., 1980). However, standard gastruloid protocols culture them as free-floating aggregates (Van den Brink et al., 2014), preventing substrate attachment and limiting morphogenetic forces to cell-cell interactions (Hashmi et al., 2022; Oriola et al., 2024; Fiuza et al., 2024; Gsell et al., 2025; McNamara et al., 2024). Alternatively, in 2D gastruloid models cell-substrate interactions are introduced using micropatterning techniques to grow embryonic stem cells on matrix-coated spots of defined size and shape, where germ layers form robust concentric ring patterns (Warmflash et al., 2014; Morgani et al., 2018). Micropatterning enables precise control over gastruloid geometry and mesoderm induction sites (Muncie et al., 2020); however, the confined nature, flat geometry and adhesive coatings presumably restrict morphogenetic movements, preventing the formation of a patterned body axis characteristic of their three-dimensional counterparts. For these reasons, how ECM dynamics regulate cellular behaviours and direct morphogenetic strategies remains unexplored in gastruloid systems. Here, we explore how gastruloids undergo morphogenesis when cultured on different substrates without micropatterned constraints. Using systematic ECM coatings combined with quantitative morphological analysis and chemical perturbations of key cytoskeletal components, we demonstrate that distinct extracellular environments direct unique morphogenetic mechanisms involving diverse cellular behaviours and likely force generation strategies. Our results reveal that gastruloids can plastically respond to their external environment, achieving axial elongation through distinct strategies.

Results

Mesoderm specification regulates gastruloid substrate-adhesion profile

Morphogenetic processes such as cell migration, epithelial folding, and tissue elongation require mechanical forces generated through cell-cell or cell-substrate interactions. In standard gastruloid culture, cells aggregate in ultra-repellent plastic wells that prevent substrate attachment (Van den Brink et al., 2014), creating a system where morphogenesis relies mostly on cell-cell interactions to generate forces.

Here we probed the developmental potential of gastruloids in the presence of various adherent substrates. We developed an automated imaging pipeline to quantify the dynamics of reported gene expression, morphology, and cell migration on gastruloids cultured on ECM-coated surfaces (Fig. 1A). By day 5, gastruloids cultured on these surfaces exhibit diverse morphogenetic outcomes depending on the substrate, which differ significantly from the simple elongated shape of regular free-floating gastruloids (Fig. 1B). For instance, gastruloids growing on laminin develop multiple cell streams forming flat projections at their periphery and a halo of individually migrating cells, while gastruloids cultured on either fibronectin or collagens IV/I are characterized by a single elongating pole and variable degrees of cell migration surrounding them.

Interestingly, gastruloid adhesion preferences change over time (Fig. 1D): When exposed to ECM-coated glass surfaces after aggregation (day 2), gastruloids attach exclusively to laminin, not adhering to any other coating (fibronectin, collagen I, collagen IV); however, at later stages (day 3 - day 4), gastruloids gain the ability to adhere to all tested components, suggesting a shift in the substrate adhesion capabilities following CHIR99021 (Chiron) exposure on day 2. Since Chiron stabilises mesoderm induction and mesoderm cells exhibit a distinct adhesion profile (Burdsal et al., 1993), we hypothesised that Chiron exposure could be necessary for gastruloid cells to attach to ECM proteins other than laminin. Indeed, in the absence of Chiron exposure on day 2, gastruloids failed to attach to fibronectin and collagen IV/I coated surfaces from day 3 onward, while maintaining their ability to adhere to laminin (Fig. 1B-D, Fig. S1). Notably, free floating gastruloids not exposed to Chiron express T/Bra in a delayed fashion (Fig. 1D), but do not elongate (Fig. 1B-D, Fig. S1).

Finally, we also tested the effects of Matrigel, a basement membrane extract mainly composed of laminin and collagen IV (Sodek et al., 2008; Kibbey, 1994). However, despite the presence of laminin, we found that gastruloids on Matrigel did not replicate the phenotype observed on laminin. Instead, Matrigel induced a morphology similar to fibronectin and collagens exposed gastruloids (Fig. S2A), with the same Chiron-dependent adhesion temporal profile (Fig. S2B), which suggests that other components of the extract might have a dominant effect over the laminin at this early stage.

Overall, these results demonstrate that gastruloid adhesion profiles change with their differentiation state, possibly mirroring the sequential deposition of ECM components during embryonic development. The strong affinity for laminin, independent of Chiron treatment, possibly reflects its primordial role as the first ECM protein in mammalian embryos (Cooper and MacQueen, 1983).

Gastruloids on laminin and free-floating conditions exhibit similar fate specification abilities

In free-floating gastruloids, on day 4, the emergence of the axis is preceded by the formation of a T/Bra-positive pole from an initial salt-and-pepper pattern of T/Bra-positive cells (Van den Brink et al., 2014; Hashmi et al., 2022); followed by axial elongation on day 5, possibly driven by cell-cell interactions (Gsell et al., 2025; McNamara et al., 2024; Mayran et al., 2023). We explored whether similar T/Bra-positive cell dynamics are associated with the emergence of cell streams when gastruloids are cultured on laminin. Similar to micropatterned systems (Warmflash et al., 2014; Morgani et al., 2018), we found that T/Bra-positive cells organize as a ring on the edge of the flat gastruloid on day 3, and by day 4 they coalesce into poles (Fig. 2A). Notably, T/Bra cells on laminin tend to form multiple poles rather than coalescing into a single axis as in free-floating conditions, likely due to the geometric and motility constraints imposed by adhesion to the substrate.

Next, we examined the activation of proteins associated with morphogenetic movements. We observed that the emerging cell streams on laminin are associated with a striking pattern of myosin activation (Fig. 2B) where double-phosphorylated (2-P) myosin is highly enriched in the elongating stream and completely absent in the main body of the gastruloid. Instead, in free-floating gastruloids, 2-P myosin shows a diffuse pattern without distinct domains (Fig. 2B). This suggests that elongation involves distributed tissue contributions in free-floating gastruloids, whereas on laminin it is primarily driven by T/Bra-positive cells. However, despite these differences in its activation patterns, myosin contraction is necessary for morphogenesis in both laminin-cultured and free-floating gastruloids, as demonstrated by Rho kinase inhibition, which hinders elongation in both scenarios (Fig. S3).

Beyond myosin activation, we looked at EMT markers. EMT is characterized by the downregulation of E-cadherin and the upregulation of N-cadherin and SNAI1 (Cano et al., 2000; Lamouille et al., 2014). Since this cadherin switch regulates the elongation of conventional free-floating gastruloids (Mayran et al., 2023), we investigated whether a similar transition occurs in gastruloids undergoing axial elongation on laminin. By day 5, SNAI1 is expressed in a band at the base of the cell streams, mirroring the pattern observed in free-floating gastruloids (Fig. 2C). Similarly to free-floating gastruloids, E-cadherin expression is largely lost throughout laminin-cultured gastruloids (Hashmi et al., 2022; Mayran et al., 2023; Fiuza et al., 2024), persisting only in patches, while N-cadherin is highly expressed at the

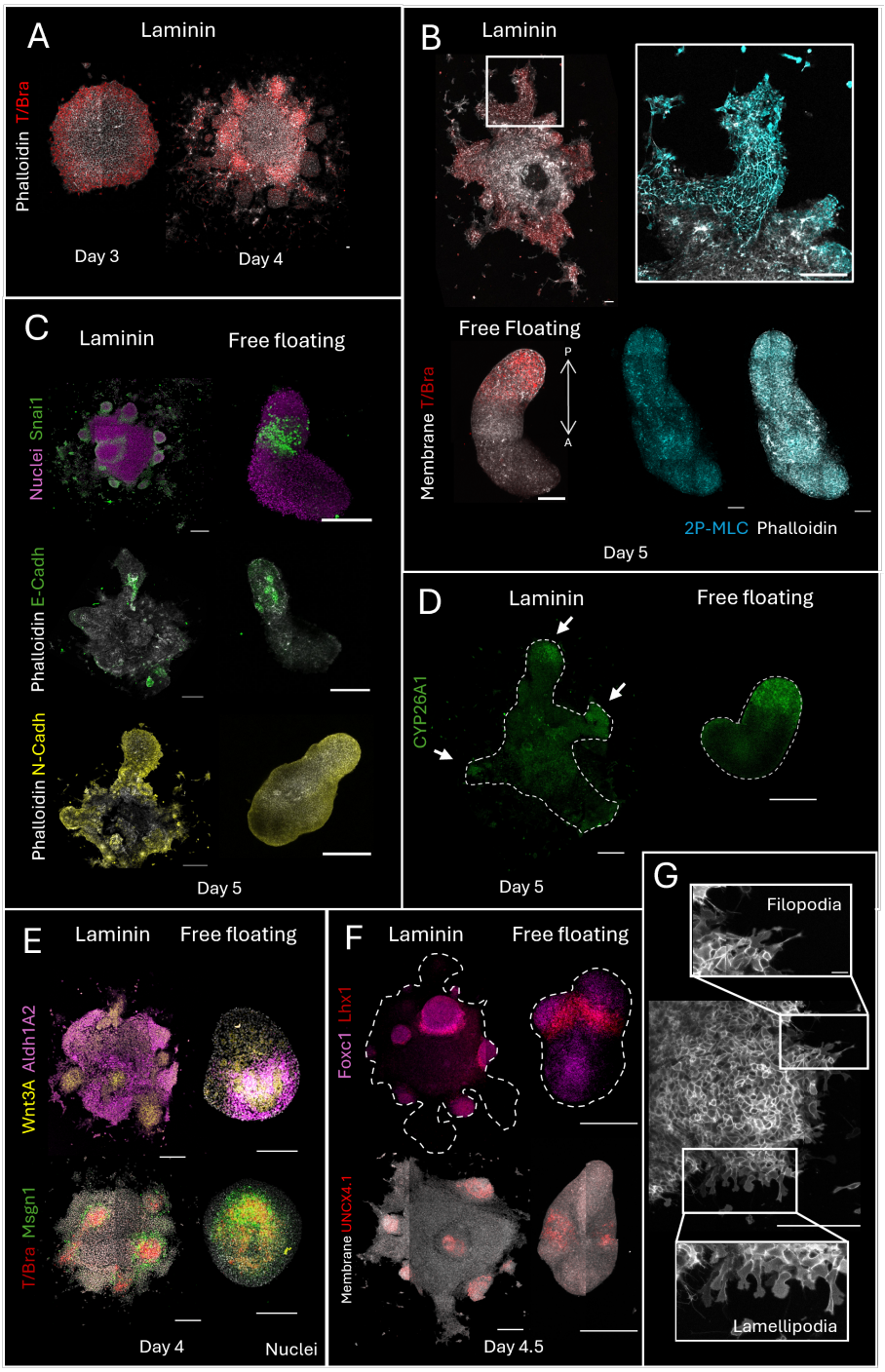

Fig. 2. Free floating and laminin gastruloids share similar differentiation abilities. A) T/Bra immunostaining of gastruloids on laminin on days 3 and 4. B) T/Bra and double phosphorylated myosin immunostaining in free-floating and laminin gastruloids on day 5. C) EMT-associated immunostainings on day 5 in free-floating and laminin gastruloids. D) Expression of the posterior tip marker CYP26A1 in in free-floating and laminin gastruloids on day 5. E) HCR for Wnt3A, Aldh1A2, T/Bra and Msgn1 in in free-floating and laminin gastruloids on day 4. E) HCR for Foxc1, Lhx1 and Uncx4.1 in free-floating and laminin gastruloids on day 4.5. G) Confocal image of a cell stream emerging in a membrane GFP gastruloid on laminin. Scale bars are 200m for the free-floating gastruloids and 500m for the laminin gastruloids.

outer edges of the gastruloid and within the cell streams (Fig. 2C). These results indicate that free-floating gastruloids and gastruloids on laminin undergo a comparable EMT.

We then tested whether gastruloids on laminin can generate the hallmarks of a patterned posterior body axis beyond T/Bra expression as in free-floating gastruloids. In free-floating gastruloids and embryos, the most posterior tip expresses Cyp26a1, an enzyme involved in RA catabolism. Similarly, the distal ends of cell streams on laminin express Cyp26a1 (Fig. 2D, Fig. S4), indicating their patterned posterior identity. Consistent with

this, we observed the expected anterior-posterior segregation pattern: Wnt3a (posterior marker) is localized in the cell streams, while Aldh1a2 (anterior RA synthesis marker) is expressed in the main body of the gastruloid (Fig. 2E). These findings demonstrate that cell streams possess the molecular hallmarks of posterior tissues and that gastruloids on laminin can establish proper axis patterning. Lastly, we confirmed that posterior identities are necessary for cell stream formation by shifting gastruloid tissues towards more anterior fates using activin A, instead of Chiron (Dias et al., 2025). In these conditions, free-floating and laminin gastruloids fail in elongation, indicating that cell stream formation indeed depends on the presence of posterior cell fates (Fig. S5).

Furthermore, we observed enhanced spatial separation of mesodermal derivatives when gastruloids are cultured on laminin. This includes distinct localisation of early (Msgn1, Fig. 2E) and late (Foxc1, Uncx4.1, Fig. 2F) paraxial mesoderm markers, and intermediate mesoderm markers (Lhx1, Fig. 2F). Notably, gastruloids on laminin can form bulging structures that often flank the cell streams and express somite-associated markers (Foxc1, Uncx4.1, Fig. 2F) in organized clusters, contrasting with the more sparsely distributed expression observed in free-floating gastruloids (Fig. 2F). This enhanced organization supports the idea that laminin promotes somitogenesis in gastruloids, consistent with previous studies using Matrigel to induce somite-like structures (Van Den Brink et al., 2020; Veenvliet et al., 2020).

Finally, we performed live imaging using a line expressing EGFP at the cell membrane (GPI-GFP, see methods) to capture the cellular behaviors associated with cell stream elongation (Movie 1). Remarkably, we observed that the emergence of the streams was a highly dynamic process, characterized by the active protrusion of filopodia and lamellipodia around the cell streams (Fig. 2B).

Inhibition of lamellipodia formation enhances collective cell migration on laminin

We hypothesised that these highly dynamic protrusions could play a role in the elongation process. To specifically assess the role of lamellipodia in the elongation of cell streams on laminin, we used CK666 (Fig. 3), an inhibitor of the Arp2/3 complex (Hetrick et al., 2013; Nolen et al., 2009). This complex is an actin nucleator that organizes actin fibers in a branching configuration necessary for lamellipodia formation (Mullins et al., 1998; Goley and Welch, 2006). As expected, adding CK666 between days 4 and 5 reduced the formation of lamellipodia activity (Fig. S6) and the individual cell migration on both laminin and fibronectin (Fig. 3A-B, Fig. S7A), suggesting that lamellipodia are required for the effective directed displacement of individual cells. Surprisingly, however, CK666 treatment resulted in longer cell streams protruding only from gastruloids on laminin (Fig. 3C, E), with no measurable effect on the elongation of free-floating gastruloids or those seeded on fibronectin (Fig. S7).

Curiously, CK666 produced no measurable differences in free-floating gastruloids (Fig. 3B). For a more detailed analysis of the final shape, we decomposed the gastruloid morphology using LOCO-EFA modes (Fig. S67), a series of unbiased bidimensional shape descriptors based on Fourier transforms (Sánchez-Corrales et al., 2018). While the contributions of the first two modes describe ellipsoidal shapes, higher frequencies are necessary to characterize more complex or extreme morphologies. This analysis revealed that CK666 treatment did not alter the morphology of free-floating gastruloids or those seeded on fibronectin, but shifted laminin-seeded gastruloids toward more complex, elongated anatomies (Fig. S7C).

Next, we sought to identify the underlying cause of the more elongated morphology. Since there was no change in the area of laminin-seeded gastruloids after CK666 treatment (Fig. S7), we hypothesized that the elongation resulted from enhanced migration capabilities of cell streams (Movie 2). To test this, we quantified the migration speed of cell stream tips from gastruloids on laminin exposed to CK666 (Movie 3). Our measurements revealed that migration velocity increased, confirming that inhibition of the Arp2/3 complex enhanced their migratory capacity (Fig. 3D).

To further investigate the tissue movements, we recorded high-resolution time-lapse movies of protrusion formation using the GPI-GFP line with or without CK666. Particle image velocimetry (PIV) analysis of these movies suggested that cells move in a coherent directional manner with an increased velocity in the presence of CK666 (Fig. 3F, Fig. S8). In both conditions, we did not observe significant oriented cell intercalations once cells abandoned gastruloid's main body and entered the stream, which suggests that the formation of these streams represents a form of collective cell migration rather than convergent-extension fuelled by oriented cell intercalations. The pattern of tissue flows was not affected by the addition of CK666, except for the enhanced migration speed.

Finally, we observed that cell divisions in the "neck" of the cell stream (the stalk connecting the most distal -posterior- tip with the main gastruloid body) preferentially orient perpendicular to the elongation axis (Fig. 3G). We hypothesised that lamellipodia at the perimeter of the stream (Fig. 2G) generate lateral pulling forces that bias cell division angles (Fig. 3G). These perpendicular forces are presumably counterproductive for the cell stream formation since they contribute to lateral rather than axial elongation. Strikingly, CK666 treatment caused cell division orientation to shift and statistically align with the elongation axis (Fig. 3G), suggesting that removing lamellipodia reduces lateral pulling, leaving only productive forces that promote axial elongation, increasing migration speed.

Filopodia are required for cell stream formation on laminin

Having established that inhibiting lamellipodia formation enhances collective cell migration and stream elongation specifically on laminin, we next investigated the role of filopodia in this process. Filopodia are finger-like cellular protrusions composed of parallel bundles of actin filaments (Mattila and Lappalainen, 2008), which

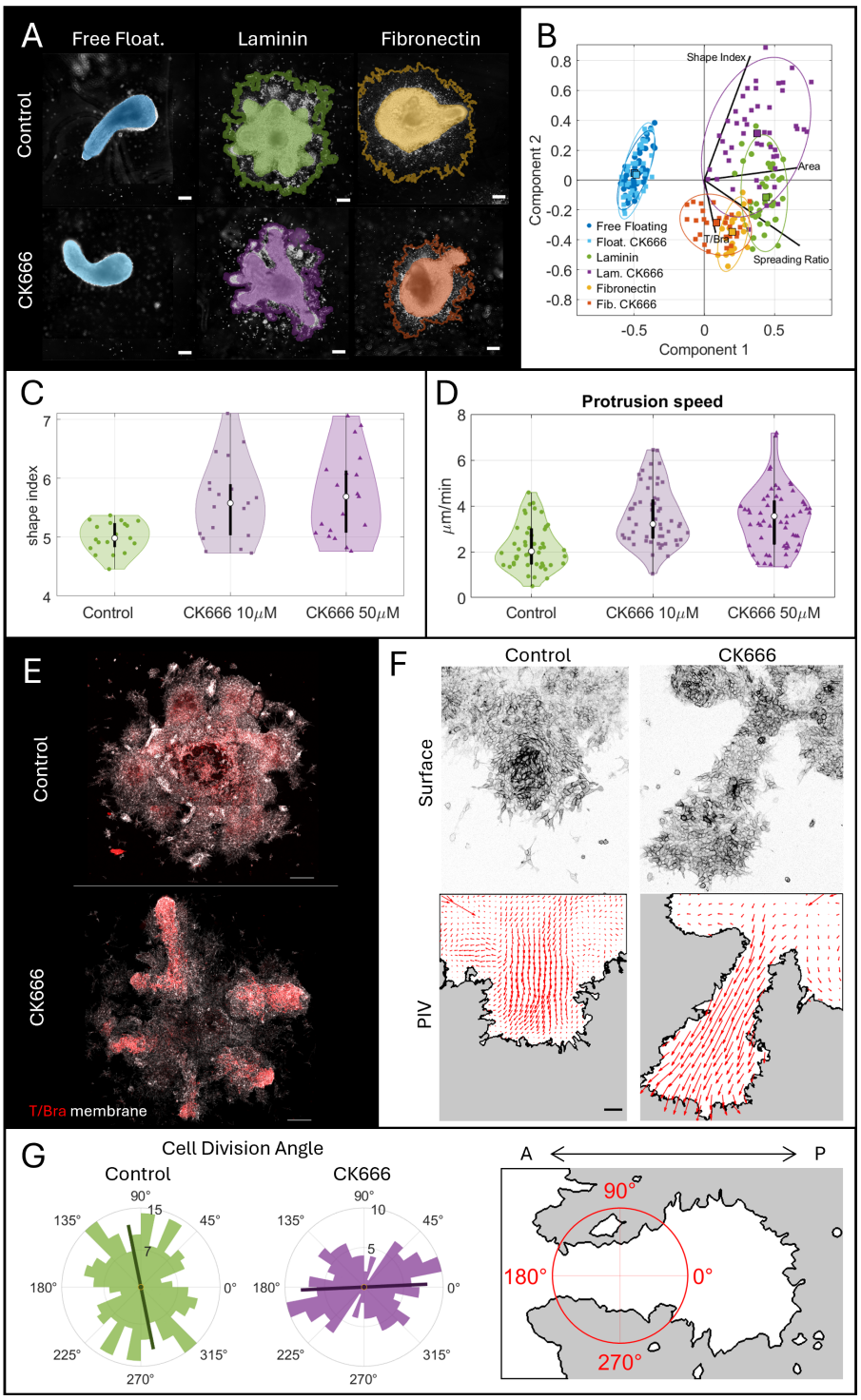

Fig. 3. Inhibition of lamellipodia enhances elongation on laminin-seeded but not on free-floating gatruloids A) Gastruloid morphologies on different substrates with or without CK666 $50\mu M$ at day 5. B) Principal Component Analysis integrating different properties on day 5 (see Fig. S7A). C) Quantification of the shape-index with different CK666 concentrations. D) Quantification of the migration speed of T/Bra positive tips E) High-resolution image demonstrating the higher elongation capabilities of laminin-seeded gastruloids treated with CK666. F) Particle image velocimetry on the developing cell streams (see Fig. S8). G) Quantification of the cell division angle with respect to axis of elongation. See supplementary material for full statistical analysis. Colours indicate the same conditions across graphs. Scale bars are $200\mu m$ in A-E and $50\mu m$ in F.

are primarily nucleated by Formin proteins (Courtemanche, 2018). To determine whether these actin-rich protrusions are required for the laminin-specific cell stream elongation (Fig. 4), we treated gastruloids with SMIFH2, a small molecule inhibitor of Formin homology 2 domains (Rizvi et al., 2009), producing a reduction in filopodial length, on laminin (Fig. S6) and free-floating (Fig. S9) gastruloids.

Strikingly, SMIFH2 blocked the formation of cell streams in a dose-dependent manner, or with increased exposure time, on laminin-seeded gastruloids, while having no effect on their free-floating counterparts (Fig. 4). The inhibitor prevented area expansion, individual cell migration, and cell stream formation in gastruloids cultured on laminin (Fig. S10A), but had no measurable effect on free-floating gastruloids as shown in the integrated PCA (Fig. 4B). Indeed, LOCO-EFA shape analysis demonstrated that SMIFH2 decreased the morphological complexity of laminin-seeded gastruloids in a dose-dependent manner (Fig. S10B). While control gastruloids on laminin developed complex shapes characterized by higher-order LOCO-EFA modes, SMIFH2-treated gastruloids remained predominantly circular (Fig. S10C).

We did not observe significant changes in mesodermal differentiation (T/Bra), the cadherin switch (E-cadherin/N-cadherin), or the specification of anteroposterior markers (Aldh1A2/Wnt3a) upon addition of SMIFH2 at day 3.5 (84 hours), even at the highest tested concentration (25 μM, Fig. 4D, Fig. S10D). This suggests that filopodia inhibition does not substantially affect signalling pathways, but instead plays a critical mechanical role in generating forces on a substrate. Moreover, if filopodia were significantly involved in signalling, we would expect to see similar effects in free-floating gastruloids, which also exhibit filopodial protrusions (Fig. S9). Altogether, these results demonstrate that filopodia are essential for the formation and elongation of cell streams in laminin-seeded gastruloids (Movie 4). The absence of SMIFH2 effects in free-floating gastruloids (Fig. 4), combined with our findings from CK666 experiments (Fig. 3), suggests that gastruloids can employ distinct mechanisms for axis elongation depending on their physical environment.

Discussion

Our findings reveal that gastruloids present a temporal cell-substrate adhesion profile that mirrors the sequential deposition of ECM components in the embryo. Gastruloids show strong affinity for laminin from the time of aggregation, independent of Chiron treatment. This likely reflects the primordial role of laminin in mammalian gastrulation: it is the first ECM protein to appear in mammalian embryos (Leivo et al., 1980; Cooper and MacQueen, 1983) and the only ECM component whose absence results in lethal phenotypes during gastrulation (Schéele et al., 2007). In contrast, the delayed, Chiron-dependent adhesion to fibronectin and collagens IV/I (Leivo et al., 1980) may reflect the requirement for mesoderm-associated EMT and subsequent ECM-specific integrin expression (Burdsal et al., 1993).

Early attachment to laminin before or during Chiron treatment constrains gastruloid morphogenesis, preventing the formation of a single body axis. While free-floating gastruloids consolidate mesoderm precursors into a single pole through extensive cell rearrangements (Hashmi et al., 2022; Gsell et al., 2025), laminin-adherent gastruloids develop multiple body axes. This multipolar morphology possibly arises because strong cell-substrate adhesion restricts cell mobility during days 2-4, trapping T/Bra-positive cells at their sites of induction around the gastruloid periphery. Unable to coalesce through collective rearrangements, each cluster of mesoderm precursors instead initiates local axis elongation, transforming what would be a single posterior pole into multiple radiating streams. Each of these streams is capable of establishing a patterned anteroposterior axis, providing new evidence for the relative independence of the morphogenetic and transcriptional programs (Bennabi et al., 2024; Merle et al., 2024). By day 4, mesoderm cells have acquired the molecular machinery necessary for substrate-based migration, enabling the transformation of mesoderm cell clusters into actively elongating streams. This morphogenetic process shows specific cytoskeletal requirements: filopodia are essential for stream formation, while lamellipodia paradoxically restrict elongation efficiency. In contrast, free-floating gastruloids are unaffected by inhibition of either formins or Arp2/3, indicating they employ fundamentally different elongation mechanisms. Although substrate-adherent gastruloids harness cell-ECM traction to drive morphogenesis, their free-floating counterparts most probably rely on cell-cell-generated forces, likely through differential adhesion and cortical contractility, to achieve axis elongation (McNamara et al., 2024; Mayran et al., 2023; Fiuza et al., 2024; Oriola et al., 2024).

Similar cytoskeletal dependencies have been observed in cancer cell migration. Arp2/3 inhibition increases linear migration velocity in rat glioma cells, while formin inhibition blocks migration entirely (Monzo et al., 2016). Additionally, formins appear essential for EMT in lung, mammary, and renal epithelial cells, where SMIFH2 treatment prevents SMAD2 phosphorylation and subsequent EMT-associated changes (Rana et al., 2018). However, we observed no changes in EMT marker expression following SMIFH2 treatment in either laminin-adherent or free-floating gastruloids.

Together, these observations might point to a primarily mechanical function for filopodia in our system. Focal adhesions can form at filopodia tips during collective cell migration (Bischoff et al., 2021), providing the mechanical anchorage necessary for force transmission. The absence of EMT marker changes following SMIFH2 treatment, combined with the lack of morphological effects in free-floating gastruloids, argues against essential signalling roles for filopodia in mesoderm specification or maintenance. If filopodia-mediated signalling were critical for these processes, we would expect formin inhibition to disrupt morphogenesis regardless of substrate availability. Instead, the strictly substrate-dependent phenotype suggests that filopodia could function mostly as mechanical effectors, required only when cells must generate traction against an ECM substrate.

Recent reports demonstrate that T/Bra-positive cells within free-floating gastruloids generate active protrusions (Anlaş et al., 2024), which are likely dependent on non-canonical Wnt signalling (Fiuza et al., 2024). Furthermore, blocking non-canonical Wnt prevents the coalescence of T/Bra clusters (Fiuza et al., 2024), suggesting that this pathway is necessary for the mechanical changes driving mesoderm progenitor sort-

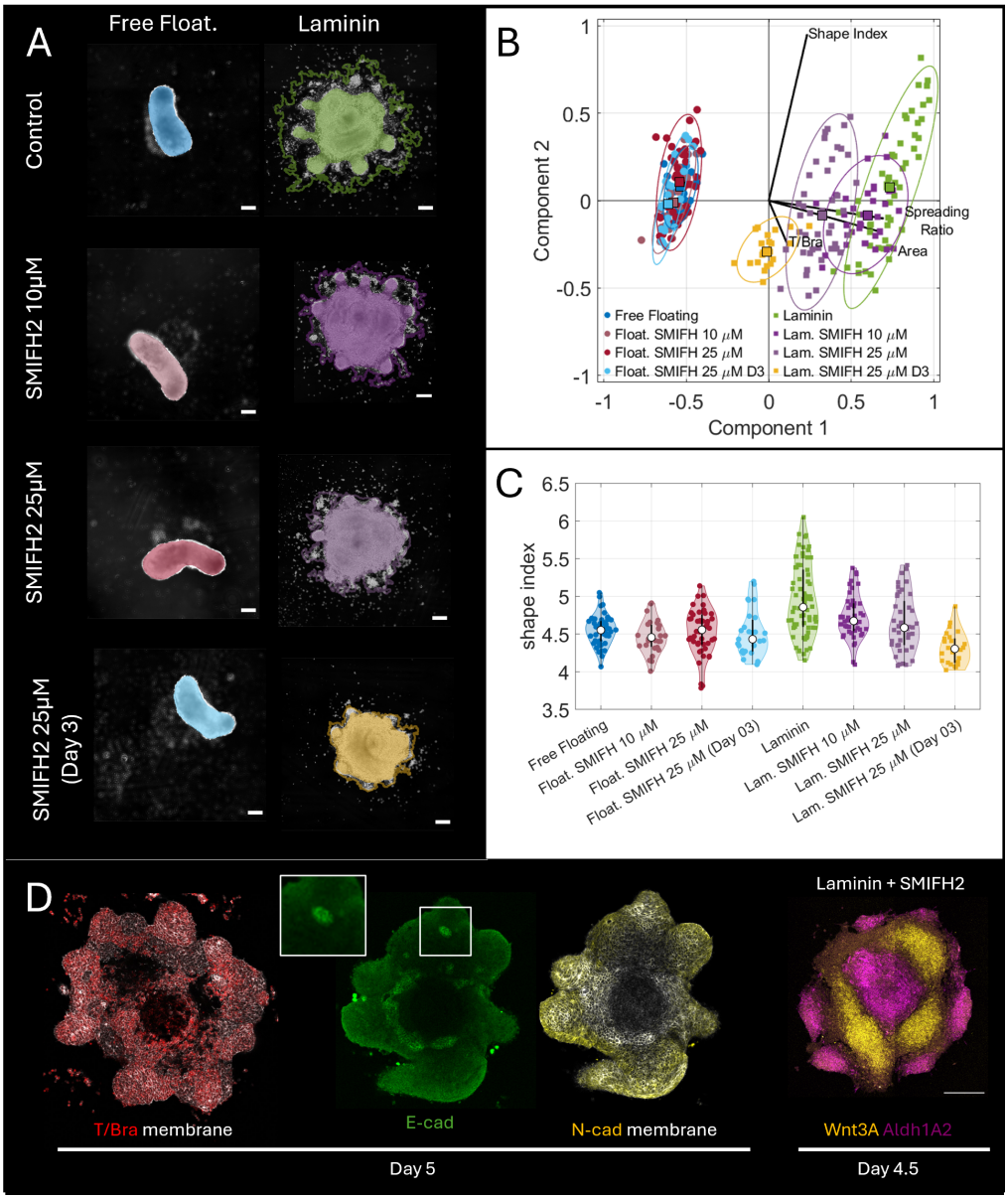

Fig. 4. Inhibition of filopodia blocks elongation on laminin-seeded but not on free-floating gatruloids A) Gastruloid morphologies on different substrates with or without SMIFH2 at day 5. B) Principal Component Analysis integrating different properties on day 5 (see Fig. S10A). C) Quantification of the shape-index with different SMIFH2 concentrations. D) Expression of T/Bra (reporter line), E/N-Cadherins (immunofluorescence), and Wnt3/Aldh1A2 (HCR) on laminin gastruloids treated with SMIFH2 25μM at day 3 (84h). Inset shows a patch of E-Cadherin expression on the cell membrane. See supplementary material for full statistical analysis. Colours indicate the same conditions across graphs. Scale bars are 200μm.

ing and subsequent axis formation. Indeed, previous studies have demonstrated that filopodia are necessary for non-canonical Wnt-induced cell migration (Nishita et al., 2006). These reports, together with the data presented here, suggest that non-canonical Wnt induces an excitable cytoskeleton that generates cell protrusions (filopodia and lamellipodia) and alters mechanical properties, ultimately driving tissue elongation through cell-cell interactions in free-floating conditions or cell-substrate interactions when adherent to ECM.

Here we show that gastruloid morphology is plastic and can be reshaped under different circumstances. Developmental plasticity could serve as raw material for evolution, allowing organisms to explore alternative developmental trajectories without compromising essential gene regulatory networks. Morphogenetic flexibility manifests when environmental, extraembryonic, or maternal inputs reshape embryonic development, as recently demonstrated (Chuai et al., 2023; Serra et al., 2023; Urbansky et al., 2016). These extrinsic inputs can trigger integrated developmental adjustments that produce viable phenotypes through a process called phenotypic accommodation (West-Eberhard, 2005). This type of accommodation has been observed in the sea anemone *Nematostella vectensis*, which undergoes gastrulation through either invagination or cell ingression followed by cavitation, depending on the geometric constraints (Kirillova et al., 2018). Most generally, gastru-

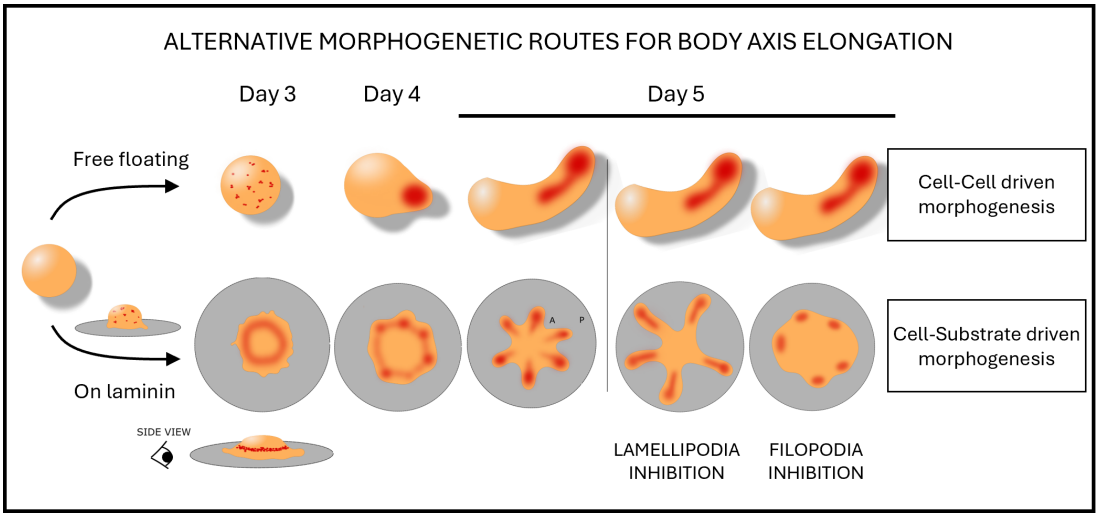

Fig. 5. Adherent substrates reveal different morphogenetic routes to generate a posterior body axis in gastruloids. Summary of the findings: When grown on an adhesive substrate, gastruloids undergo body axis elongation using cell-substrate interactions regulated by lamellipodia and filopodia. Instead, free-floating gastruloids elongate using cell-cell interactions that do not depend on cellular protrusions

lation in cnidarians seems more dependent on variable features like egg size and maternal provisioning than on evolutionary history (Kraus and Markov, 2017), suggesting that plastic developmental properties are basal in animal evolution.

Our results show that mammalian development retains significant plasticity, which can be revealed in vitro under appropriate conditions. This developmental flexibility provides a mechanism for the diversification of early embryonic strategies in response to changes in maternal conditions, egg properties, or other environmental factors; potentially providing an explanation for the widening of the base of the vertebrate developmental hourglass pattern (Steventon et al., 2021). In other words, developmental plasticity could allow for environmentally induced alternative morphologies and gastrulation modes (Serrano Nájera and Weijer, 2023), while maintaining essential patterning programs and a similar body plan. Supporting this model, anamniote embryo explants (teleost and amphibian) develop elongated morphologies similar to mammalian gastruloids when separated from their original environment (Thomsen et al., 1990; Fulton et al., 2020), suggesting a similar morphogenetic potential that is reshaped by external conditions.

Our findings suggest that the embryo could accommodate substrate-induced morphological variations. By maintaining core patterning programs while deploying different morphogenetic mechanisms, developing tissues preserve essential functions while exploring morphological space. This flexibility could enable evolutionary diversification, as environmentally-revealed developmental variants provide targets for selection without requiring immediate genetic change. More broadly, the capacity for plastic phenotypic accommodation challenges deterministic views of morphogenesis and suggests that evolutionary innovations may arise not from new genetic programs (West-Eberhard, 2005), but from environmentally induced developmental variations that reveal latent mechanical capabilities. Finally, these experiments expose what types of processes should be characterised *in vivo*.

In conclusion, our work demonstrates the ability of gastruloids to achieve body axis elongation using different morphogenetic strategies depending on context. On the practical side, these findings have important implications for tissue engineering and organoid technologies, suggesting that desired morphologies might be achieved through multiple mechanical routes, and broader implications for understanding birth defects that may result from inappropriate mechanical contexts during development.

Acknowledgments

GSN acknowledges support from Leverhulme Trust Early Career Fellowship (ECF-2022-474). AD and BJS acknowledges support from the a Wellcome Trust Discovery Award (225360/Z/22/Z). We thank the Steventon lab members, and Marta Urbanska for their support and enlightening discussion. Imen Lassadi and Oskar Batty for sharing of the SBN line.

Author contributions

CRediT taxonomy terms for the individual contributions.

GSN: Conceptualisation, Software, Validation, Formal Analysis, Investigation, Data Curation, Writing – Original Draft, Visualisation, Supervision, Funding acquisition. AD: Validation, Formal Analysis, Investigation, Data Curation, Writing – Original Draft, Visualisation. BJS: Conceptualisation, Resources, Project administration, Funding acquisition.

References

Anand, G. M., Megale, H. C., Murphy, S. H., Weis, T., Lin, Z., He, Y., Wang, X., Liu, J., and Ramanathan, S. (2023). Controlling organoid symmetry breaking uncovers an excitable system underlying human axial elongation. *Cell*, 186(3):497–512.

Anlaş, K., Gritti, N., Nakaki, F., Salamó Palau, L., Tlili, S. L., Oriola, D., Arató, K., Le Lim, J., Sharpe, J., and Trivedi, V. (2024). Early autonomous patterning of the anteroposterior axis in gastruloids. *Development*, 151(22).

Anlas, K. and Trivedi, V. (2021). Studying evolution of the primary body axis in vivo and in vitro. *Elife*, 10:e69066.

Bennabi, I., Hansen, P., Merle, M., Pineau, J., Lopez-Delisle, L., Kolly, D., Duboule, D., Mayran, A., and Gregor, T. (2024). Size-dependent temporal decoupling of morphogenesis and transcriptional programs in gastruloids. *bioRxiv*, pages 2024–12.

Bischoff, M. C., Lieb, S., Renkawitz-Pohl, R., and Bogdan, S. (2021). Filopodia-based contact stimulation of cell migration drives tissue morphogenesis. *Nature communications*, 12(1):791.

Burdsal, C. A., Damsky, C. H., and Pedersen, R. A. (1993). The role of e-cadherin and integrins in mesoderm differentiation and migration at the mammalian primitive streak. *Development*, 118(3):829–844.

Cano, A., Pérez-Moreno, M. A., Rodrigo, I., Locascio, A., Blanco, M. J., del Barrio, M. G., Portillo, F., and Nieto, M. A. (2000). The transcription factor snail controls epithelial–mesenchymal transitions by repressing e-cadherin expression. *Nature cell biology*, 2(2):76–83.

Chuai, M., Serrano Nájera, G., Serra, M., Mahadevan, L., and Weijer, C. J. (2023). Reconstruction of distinct vertebrate gastrulation modes via modulation of key cell behaviors in the chick embryo. *Science Advances*, 9(1):eabn5429.

Cooper, A. R. and MacQueen, H. A. (1983). Subunits of laminin are differentially synthesized in mouse eggs and early embryos. *Developmental biology*, 96(2):467–471.

Courtemanche, N. (2018). Mechanisms of formin-mediated actin assembly and dynamics. *Biophysical reviews*, 10(6):1553–1569.

del Corral, R. D. and Storey, K. G. (2004). Opposing fgf and retinoid pathways: a signalling switch that controls differentiation and patterning onset in the extending vertebrate body axis. *Bioessays*, 26(8):857–869.

Dias, A., Pascual-Mas, P., Robertson, G., Torregrosa-Cortés, G., Stelloo, S., Casani-Galdón, P., Babin, S., Romaniuk, Y., Mayran, A., Wehmeyer, A. E., Garcia-Ojalvo, J., McNamara, H. M., Vermeulen, M., Arnold, S. J., and Martinez Arias, A. (2025). Opposing nodal and wnt signalling activities govern the emergence of the mammalian body plan. *bioRxiv*, pages 2025–01.

Fiuza, U.-M., Bonavia, S., Pascual-Mas, P., Torregrosa-Cortes, G., Casani-Galdon, P., Robertson, G., Dias, A., and Martinez Arias, A. (2024). Morphogenetic constrains in the development of gastruloids: implications for mouse gastrulation. *bioRxiv*, pages 2024–12.

Fulton, T., Trivedi, V., Attardi, A., Anlas, K., Dingare, C., Arias, A. M., and Steventon, B. (2020). Axis specification in zebrafish is robust to cell mixing and reveals a regulation of pattern formation by morphogenesis. *Current Biology*, 30(15):2984–2994.

Goley, E. D. and Welch, M. D. (2006). The arp2/3 complex: an actin nucleator comes of age. *Nature Reviews Molecular Cell Biology*, 7(10):713–726.

Gsell, S., Tlili, S., Merkel, M., and Lenne, P.-F. (2025). Marangoni-like tissue flows enhance symmetry breaking of embryonic organoids. *Nature Physics*, pages 1–10.

Hashmi, A., Tlili, S., Perrin, P., Lowndes, M., Peradziryi, H., Brickman, J. M., Arias, A. M., and Lenne, P.-F. (2022). Cell-state transitions and collective cell movement generate an endoderm-like region in gastruloids. *Elife*, 11:e59371.

Hetrick, B., Han, M. S., Helgeson, L. A., and Nolen, B. J. (2013). Small molecules ck-666 and ck-869 inhibit actin-related protein 2/3 complex by blocking an activating conformational change. *Chemistry & biology*, 20(5):701–712.

Kibbey, M. C. (1994). Maintenance of the ehs sarcoma and matrigel preparation. *Journal of tissue culture methods*, 16:227–230.

Kirillova, A., Genikhovich, G., Pukhlyakova, E., Demilly, A., Kraus, Y., and Technau, U. (2018). Germ-layer commitment and axis formation in sea anemone embryonic cell aggregates. *Proceedings of the National Academy of Sciences*, 115(8):1813–1818.

Kraus, Y. A. and Markov, A. (2017). Gastrulation in cnidaria: The key to an understanding of phylogeny or the chaos of secondary modifications? *Biology Bulletin Reviews*, 7:7–25.

Kyprianou, C., Christodoulou, N., Hamilton, R. S., Nahaboo, W., Boomgaard, D. S., Amadei, G., Migeotte, I., and Zernicka-Goetz, M. (2020). Basement membrane remodelling regulates mouse embryogenesis. *Nature*, 582(7811):253–258.

Lamouille, S., Xu, J., and Derynck, R. (2014). Molecular mechanisms of epithelial–mesenchymal transition. *Nature reviews Molecular cell biology*, 15(3):178–196.

Leivo, I., Vaheri, A., Timpl, R., and Wartiovaara, J. (1980). Appearance and distribution of collagens and laminin in the early mouse embryo. *Developmental biology*, 76(1):100–114.

Leptin, M. (2005). Gastrulation movements: the logic and the nuts and bolts. *Developmental cell*, 8(3):305–320.

Martins-Costa, C., Wilson, V., and Binagui-Casas, A. (2024). Neuromesodermal specification during head-to-tail body axis formation. *Current topics in developmental biology*, 159:232–271.

Mattila, P. K. and Lappalainen, P. (2008). Filopodia: molecular architecture and cellular functions. *Nature reviews Molecular cell biology*, 9(6):446–454.

Mayran, A., Kolly, D., Lopez-Delisle, L., Romaniuk, Y., Leonardi, M., Cossy, A.-C., Lacroix, T., Amândio, A. R., Osteil, P., and Duboule, D. (2023). Cadherins modulate the self-organizing potential of gastruloids. *bioRxiv*, pages 2023–11.

McNamara, H. M., Solley, S. C., Adamson, B., Chan, M. M., and Toettcher, J. E. (2024). Recording morphogen signals reveals mechanisms underlying gastruloid symmetry breaking. *Nature cell biology*, 26(11):1832–1844.

Merle, M., Friedman, L., Chureau, C., Shoushtarizadeh, A., and Gregor, T. (2024). Precise and scalable self-organization in mammalian pseudo-embryos. *Nature Structural & Molecular Biology*, 31(6):896–902.

Monzo, P., Chong, Y. K., Guetta-Terrier, C., Krishnasamy, A., Sathe, S. R., Yim, E. K., Ng, W. H., Ang, B. T., Tang, C., Ladoux, B., et al. (2016). Mechanical confinement triggers glioma linear migration dependent on formin fhod3. *Molecular biology of the cell*, 27(8):1246–1261.

Morales, J. S., Raspopovic, J., and Marcon, L. (2021). From embryos to embryoids: How external signals and self-organization drive embryonic development. *Stem cell reports*, 16(5):1039–1050.

Morgani, S. M., Metzger, J. J., Nichols, J., Siggia, E. D., and Hadjantonakis, A.-K. (2018). Micropattern differentiation of mouse pluripotent stem cells recapitulates embryo regionalized cell fate patterning. *Elife*, 7:e32839.

Mullins, R. D., Heuser, J. A., and Pollard, T. D. (1998). The interaction of arp2/3 complex with actin: nucleation, high affinity pointed end capping, and formation of branching networks of filaments. *Proceedings of the National Academy of Sciences*, 95(11):6181–6186.

Muncie, J. M., Ayad, N. M., Lakins, J. N., Xue, X., Fu, J., and Weaver, V. M. (2020). Mechanical tension promotes formation of gastrulation-like nodes and patterns mesoderm specification in human embryonic stem cells. *Developmental cell*, 55(6):679–694.

Nakaya, Y., Sukowati, E. W., Wu, Y., and Sheng, G. (2008). Rhoa and microtubule dynamics control cell–basement membrane interaction in emt during gastrulation. *Nature cell biology*, 10(7):765–775.

Nishita, M., Yoo, S. K., Nomachi, A., Kani, S., Sougawa, N., Ohta, Y., Takada, S., Kikuchi, A., and Minami, Y. (2006). Filopodia formation mediated by receptor tyrosine kinase ror2 is required for wnt5a-induced cell migration. *The Journal of cell biology*, 175(4):555–562.

Nolen, B., Tomasevic, N., Russell, A., Pierce, D., Jia, Z., McCormick, C., Hartman, J., Sakowicz, R., and Pollard, T. (2009). Characterization of two classes of small molecule inhibitors of arp2/3 complex. *Nature*, 460(7258):1031–1034.

Oriola, D., Torregrosa-Cortés, G., Arató, K., Fernández-Munuera, D., Hahn, E. M., Anlaş, K., Garcia-Ojalvo, J., and Trivedi, V. (2024). Cell-cell communication controls the timing of gastruloid symmetry-breaking. *bioRxiv*, pages 2024–12.

Rana, M. K., Aloisio, F. M., Choi, C., and Barber, D. L. (2018). Formin-dependent tgf-β signaling for epithelial to mesenchymal transition. *Molecular biology of the cell*, 29(12):1465–1475.

Rizvi, S. A., Neidt, E. M., Cui, J., Feiger, Z., Skau, C. T., Gardel, M. L., Kozmin, S. A., and Kovar, D. R. (2009). Identification and characterization of a small molecule inhibitor of formin-mediated actin assembly. *Chemistry & biology*, 16(11):1158–1168.

Sánchez-Corrales, Y. E., Hartley, M., Van Rooij, J., Marée, A. F., and Grieneisen, V. A. (2018). Morphometrics of complex cell shapes: lobe contribution elliptic fourier analysis (loco-efa). *Development*, 145(6):dev156778.

Schéele, S., Nyström, A., Durbeej, M., Talts, J. F., Ekblom, M., and Ekblom, P. (2007). Laminin isoforms in development and disease. *Journal of molecular medicine*, 85:825–836.

Serra, M., Serrano Nájera, G., Chuai, M., Plum, A. M., Santhosh, S., Spandan, V., Weijer, C. J., and Mahadevan, L. (2023). A mechanochemical model recapitulates distinct vertebrate gastrulation modes. *Science advances*, 9(49):eadh8152.

Serrano Nájera, G. and Weijer, C. J. (2023). The evolution of gastrulation morphologies. *Development*, 150(7).

Sodek, K. L., Brown, T. J., and Ringuette, M. J. (2008). Collagen i but not matrigel matrices provide an mmp-dependent barrier to ovarian cancer cell penetration. *BMC cancer*, 8:1–11.

Steventon, B., Busby, L., and Arias, A. M. (2021). Establishment of the vertebrate body plan: Rethinking gastrulation through stem cell models of early embryogenesis. *Developmental Cell*, 56(17):2405–2418.

Stower, M. J., Diaz, R. E., Fernandez, L. C., Crother, M. W., Crother, B., Marco, A., Trainor, P. A., Srinivas, S., and Bertocchini, F. (2015). Bi-modal strategy of gastrulation in reptiles. *Developmental Dynamics*, 244(9):1144–1157.

Thomsen, G., Woolf, T., Whitman, M., Sokol, S., Vaughan, J., Vale, W., and Melton, D. (1990). Activins are expressed early in xenopus embryogenesis and can induce axial mesoderm and anterior structures. *Cell*, 63(3):485–493.

Urbansky, S., González Avalos, P., Wosch, M., and Lemke, S. (2016). Folded gastrulation and t48 drive the evolution of coordinated mesoderm internalization in flies. *Elife*, 5:e18318.

Van Den Brink, S. C., Alemany, A., van Batenburg, V., Moris, N., Blotenburg, M., Vivie, J., Baillie-Johnson, P., Nichols, J., Sonnen, K. F., Martinez Arias, A., et al. (2020). Single-cell and spatial transcriptomics reveal somitogenesis in gastruloids. *Nature*, 582(7812):405–409.

Van den Brink, S. C., Baillie-Johnson, P., Balayo, T., Hadjantonakis, A.-K., Nowotschin, S., Turner, D. A., and Martinez Arias, A. (2014). Symmetry breaking, germ layer specification and axial organisation in aggregates of mouse embryonic stem cells. *Development*, 141(22):4231–4242.

van den Brink, S. C. and van Oudenaarden, A. (2021). 3d gastruloids: a novel frontier in stem cell-based in vitro modeling of mammalian gastrulation. *Trends in cell biology*, 31(9):747–759.

Veenvliet, J. V., Bolondi, A., Kretzmer, H., Haut, L., Scholze-Wittler, M., Schifferl, D., Koch, F., Guignard, L., Kumar, A. S., Pustet, M., et al. (2020). Mouse embryonic stem cells self-organize into trunk-like structures with neural tube and somites. *Science*, 370(6522):eaba4937.

Warmflash, A., Sorre, B., Etoc, F., Siggia, E. D., and Brivanlou, A. H. (2014). A method to recapitulate early embryonic spatial patterning in human embryonic stem cells. *Nature methods*, 11(8):847–854.

West-Eberhard, M. J. (2005). Phenotypic accommodation: adaptive innovation due to developmental plasticity. *Journal of Experimental Zoology Part B: Molecular and Developmental Evolution*, 304(6):610–618.

Supplementary material

Materials and methods

All materials used are listed here.

Cell culture

mESC were cultured at 37°C, 5% CO2 in 2i LIF (N2B27 (NeuroBasal medium, DMEM F-12 no glutamine, N2 —homemade (Mulas et al., 2019)—, B27, 2-Mercaptoethanol), l-glutamine, 3µM CHIR99021, 1µM PD0325901 and 0.1µg ml-1 LIF). All lines were cultured in filter-capped tissue culture flasks coated with 0.1% gelatin. Cell culture media was changed everyday, and cells were passaged every 2 days. Cells were routinely tested for mycoplasma. See supplementary table X for compounds references.

Cell lines

The lines used in this study are the parental ES-E14TG2a, the triple reporter ES-E14TG2a containing Sox1-P2A-eGFP and Bra-P2A-mCherry (Deluz et al., 2016) modified with H2B:miRFP670 (SBN), and ES-E14TG2a with CAG::GPI-GFP (GPI-GFP) (Rhee et al., 2006).

Gastruloid culture

Gastruloids were generated following a previously published protocol (Baillie-Johnson et al., 2015). A total of 200–300 mouse embryonic stem cells (mESCs) were aggregated in $40\mu L$ of N2B27 medium supplemented with Penicillin-Streptomycin (1%) and L-glutamine (referred to as supplemented N2B27) using a cell-repellent, U-bottom 96-well plate (650970, Greiner). Cells were allowed to aggregate for 48 hours, after which $150\mu L$ of supplemented N2B27 containing $3\mu M$ CHIR99021 (CHIRON pulse) was added to each well. Gastruloids were incubated in this medium for 24 $\pm$ 2 hours, after which $150\mu L$ of medium was replaced daily with fresh supplemented N2B27. Gastruloids were maintained in culture for a total of 5 days. For the activin A (AA) experiment, the chiron pulse from the original protocol was replaced by an Activin A (100ng/mL, XXXX) pulse of 24h, from 48h to 72h.

2D gastruloid protocol

Gastruloids were generated as described above. On day 2, 35 mm glass-bottom dishes were coated with $14\mu g/mL$ Laminin 111 (L2020, Sigma) for 1 hour at 37 °C. Laminin solution is prepared by diluting the stock solution in PBS without calcium and magnesium (PBS -/-) to a final concentration of $14\mu g/mL$. Gastruloids were collected using a cut $200\mu L$ pipette tip and allowed to settle at the bottom of an Eppendorf tube for a few seconds. The medium was then carefully removed, and gastruloids were resuspended in supplemented N2B27 medium containing $3\mu M$ CHIR99021. They were subsequently transferred, using a cut tip, into the Laminin-coated dish containing fresh medium. To prevent fusion, individual gastruloids were gently separated from one another using

a cut tip. The dish was then placed in the incubator, which remained closed for at least one hour to allow for proper attachment without disturbance. After 24 hours, gastruloids typically appeared flatter. From this point, medium was changed daily as described above until day 5. In the same manner, fibronectin coating is realized by diluting Fibronectin stock solution in PBS-/- to a final concentration of 12.5µg/mL. The solution is transferred to a glass-bottom dish (400µL for a 20mm dish) and incubated for 1 hour at 37°C. Before seeding, the solution is removed from the dish and washed once with PBS-/-. For collagens coatings, solutions are kept on ice until use. Collagen I is prepared by diluting the stock solution in 0.02N acetic acid to a final concentration of 12.5µg/mL overnight at 4 °C. The solution is then added to the dish and left to incubate at RT for one hour. Dishes are rinsed twice with PBS to remove acid prior gastruloids plating. Collagen IV is prepared by diluting the stock solution in cold deionized water to a working concentration of 12.5µg/mL. The subsequent steps are identical to those described for Collagen I.

Mosaic generation

Mosaics were generated following the 3D gastruloid protocol described above but using a cell suspension composed of E14 and GPI-GFP cells. Various percentages of membrane fluorescent cells have been tried including 1%, 2.5%, and 5%. With 5% giving the best results.

Chemical perturbations

Inhibitor treatments were carried out between 84h and 96h. CK666 (SML0006-5MG, Sigma), is resuspended in DMSO at a 10mM concentration upon reception and stored at 4°C. SMIFH2 (HY-16931, MedChemExpress), is resuspended in DMSO at a 10mM concentration upon reception and stored at -80°C. GSK269962A (S7687-SEL, Selleckchem), is resuspended in DMSO at a 10mM concentration upon reception and stored at -80°C. Inhibitor concentrations are as follows: CK666 (10µM and 50µM), SMIFH2 (10 and 25µM), GSK269962A (0.1µM).

Immunofluorescence staining

Gastruloids for staining are transferred to an Eppendorf using a cut tip, they are then washed once with PBS-/- before being fixed with 4% PFA overnight at 4°C (or 3 hours at room temperature). The 2D gastruloid staining protocol is identical to the 3D protocol, except that all the steps are performed directly in the dish. On the following day, gastruloids are washed twice with PBS-/-, prewashed with PBSFT (PBS -/- with 10%FBS (F9665-500ML, ThermoFisher) and 0.2% Triton X-100), washed three times with PBSFT at room temperature (10 minutes), and incubated in PBSFT for 1h at 4°C on an orbital shaker for blocking. Primary antibody solutions are prepared in PBSFT and used to replace the blocking solution once blocking is complete. Gastruloids are incubated overnight at 4°C on an orbital shaker. For 2D gastruloids, to avoid wasting antibodies, the full dish is not filled with solution. Instead, a dome of antibody solution covering the glass part of the dish is sufficient (around 400µL for a 20mm diameter glass-bottom dish). Next day, the primary antibody solution is washed as follows: 2x5 min in PBSFT (RT), 3 x 10 min PBSFT (4°C, orbital shaker), 4x 30 min (4°C, orbital shaker). Secondary solutions are prepared in PBSFT with nuclear (Sytox / DAPI) or / and Phalloidin. PBSFT wash is replaced with secondary solutions and the tubes are covered in foil and incubated overnight at 4°C on an orbital

shaker. Next day, secondary solutions are washed as described for the primary solutions. 3D gastruloids are placed in clearing solution —Scale S4,(Hama et al., 2015)— for 24 hours before mounting. 2D gastruloids are directly imaged or stored in PBS and sodium azide (0.05%) until imaging. A list of the antibodies used in this study can be found in the supplementary materials (link?).

Hybridization Chain Reaction

Fixed gastruloids are dehydrated in methanol as follows: 5 minutes per wash at room temperature: 25% MetOH / 75% PBST (PBS -/-, 0.2% Triton X-100), 50% MetOH / 50% PBST, 75% MetOH /25% PBST, 100% MetOh twice. Gastruloids are then incubated overnight at -20°C. Next day, probe hybridization buffer is pre-warmed in the incubator and amplification buffer is brought at room temperature. Gastruloids are rehydrated with a serie of 5 minutes washes, 75% MetOH /25% PBST, 50/50, etc. Once the last wash is removed, gastruloids are pre-hybridized using warm probe hybridization buffer for 30min at 37°C. Probe solution is prepared by adding 2pmol of each probe set into hybridization buffer at 37°C, the solution is transferred to the gastruloids and incubated overnight at 37°C. Next day, pre-warm probe wash buffer in the incubator and wash the gastruloids 4 x 15min at 37°C. Wash 2 x 5 min with 5 X SSCT at room temperature. Amplification buffer is added to the gastruloids to pre-amplify (5 min, RT). Prepare hairpin solutions following supplier's recommendation and add the solution to the gastruloids, incubate overnight in the dark at room temperature. The next day, remove excess hairpins by washing 3x15 min with SCCT at room temperature. Samples can be stored at 4°C until imaging / DAPI staining overnight in PBST. All HCR probes were bought from Sigma Aldrich.

Confocal microscopy

Individual gastruloids were imaged using a Zeiss LSM700 confocal microscope, typically with a 20X objective, 0.5× zoom, and 2μm axial slicing. For *in vivo* experiments, we used a humidified incubation chamber (5% CO_2, 37°C) with a time step of 5 min for 12 h and an interval between slices of 2µm.

High-throughput microscopy

Individual gastruloids were imaged using a Nikon Eclipse Ti-E inverted bright-field microscope equipped with a motorized stage, an Orca Flash 4.0 camera, a Lumencor SPECTRA X Light Engine with internal 391/22 nm, 475/28 nm, 555/28 nm, and 635/22nm excitation filters and a humidified incubation chamber (5% CO2, 37 °C). To locate each sample, we performed tile scans of individual positions on a 96-well plate (2×2) or 35 mm glass-bottom dish (7×7) at 5X magnification. Gastruloid positions were then selected using our custom MATLAB-based tool, which enables loading of multi-point microscopy data and identification of gastruloids either manually through user selection or via optional AI-assisted detection powered by Cellpose segmentation, all through an intuitive graphical interface. Once individual gastruloid positions had been recorded, we acquired single snapshots or time-lapse images with a 20X objective, capturing phase contrast and fluorescence images with appropriate illumination channels as needed.

High-throughput image analysis

We developed a MATLAB-based computational pipeline that integrates multiple tools for the segmentation and analysis of gastruloids. We used Cellpose models (Pachitariu and Stringer, 2022) trained from scratch to detect the variable morphologies of gastruloids cultured in free-floating conditions or on ECM-coated dishes. To identify the mesenchymal migration front, we utilized probability maps from a pretrained Cellpose model (CP) to detect individual cells and extracted areas with probability > 0.35. For quantitative parameter extraction (area, elongation, circularity, fluorescence intensity, etc.), as well as the LOCO-EFA descriptors (Sánchez-Corrales et al., 2018), we fed the Cellpose segmentations and original images into MOrgAna (Gritti et al., 2021). Finally, diagnostic visualization, data representation, and statistical analysis were performed using MATLAB.

Particle Image Velocimetry

Velocity fields were computed from confocal time-lapse movies (time frame = 5 min) using PIVLab v2.56 for MATLAB (Thielicke and Sonntag, 2021) with two passes of 64x64 and 32x32 pixel interrogation windows with 50% overlap with default pre- and post-processing parameters.

Lamellipodia and Filopodia quantification

Lamellipodia were manually delineated using the polygon tool in FIJI (Schindelin et al., 2012). Individual polygon coordinates were exported using a custom ImageJ macro, and the area of each polygon (lamellipodia) was computed and visualised using MATLAB. Filopodia were measured through a similar procedure, using the free-line tool in FIJI to manually trace them.

Cell division angle quantification

Division angles between daughter cell pairs were quantified at the moment of cytokinesis using confocal time-lapse movies acquired between days 4 and 5 of gastruloid development on laminin-coated substrates. The quantification procedure involved the following steps:

1. Daughter cell pair coordinates were manually identified using the multipoint tool in FIJI, and the resulting coordinates were exported to MATLAB for analysis.
2. The main elongation axis of each cell stream was defined by drawing a line along the stream's length on the final frame of the time-lapse movie using MATLAB's drawline function.
3. Cell divisions were filtered to include only those occurring within the "neck" region of the cell stream, which was defined by manual delineation using MATLAB's drawpolygon function.
4. The angle between each cell division axis and the main elongation axis of the corresponding cell stream was calculated for all samples and experimental conditions.

Statistical Analysis

All results were compiled into matrices showing adjusted p-values for all pairwise comparisons and exported as Excel files. See the Supplementary Material to find the statistical analysis associated with each figure.

Analysis for obtained from the high-throughput analysis pipeline

Statistical analyses were performed using MATLAB using a non-parametric approach. The Wilcoxon rank-sum test (Mann-Whitney U test) was conducted between all possible group combinations. This non-parametric test ranks all observations from both groups being compared and tests whether the distributions differ significantly, making it suitable for data that may not meet the assumptions of parametric tests. To account for multiple comparisons in the pairwise testing phase, p-values were adjusted using the Bonferroni correction method, where each p-value was multiplied by the total number of pairwise comparisons and capped at 1.

Analysis of lamellipodia and filopodia

MATLAB's implementation of the Wilcoxon rank-sum test was conducted between all possible group combinations. p-values were adjusted using the Bonferroni correction method.

Analysis for cell division angle data

Cell division angle analysis was performed using circular statistics appropriate for axial data using the Circular Statistics Toolbox (Berens, 2009) for MATLAB. Division angles were measured as the angle between the division axis and a reference orientation, where angles θ and $\theta + \pi$represent the same division axis. To apply circular statistical methods to axial data, all angles were converted to circular representation by doubling ($\theta \rightarrow 2\theta$), transforming the axial period of π to a circular period of 2π. This transformation preserves the axial symmetry while enabling the use of standard circular statistical functions. To test the alignment of the distribution with a preferred direction, the V-test (Rayleigh test for a specified direction) was used to test for significant concentration around specific orientations. This non-parametric test evaluates the null hypothesis that data are uniformly distributed against the alternative hypothesis of concentration around a specified direction. We tested both groups for alignment at 0 (horizontal divisions) and $\pi/2$ (vertical divisions) orientations with respect to the elongation axis.

Computational Surface Extraction

Active myosin resides in the most apical compartment of the cells. For this reason, maximum projections may not accurately represent the apical myosin, including the myosin cables. To tackle this problem we computationally acquire a 2D surface of the most apical side of the sample. To extract the apical surface of the embryo from the confocal image volumes, we used a custom MATLAB script based on the square gradient focusing algorithm (Eskicioglu and Fisher, 1995; Serrano Nájera, 2021; Serrano Nájera et al., 2024). The steps are as follows:

1. Tile the confocal volume into columns.
2. Apply the square gradient focusing algorithm to each column to find the surface position.
3. Generate a height map by finding the depth of the fastest change in the image sharpness (peak of the second derivative) for each column.
4. Apply a smoothing filter to the height map.

5. Use the smoothed height map to section the image volume and produce a 2D image of the tissue surface.

References

Baillie-Johnson, P., Van den Brink, S. C., Balayo, T., Turner, D. A., and Arias, A. M. (2015). Generation of aggregates of mouse embryonic stem cells that show symmetry breaking, polarization and emergent collective behaviour in vitro. *Journal of visualized experiments: JoVE*, (105):53252.

Berens, P. (2009). Circstat: a matlab toolbox for circular statistics. *Journal of statistical software*, 31:1–21.

Deluz, C., Friman, E. T., Strebinger, D., Benke, A., Raccaud, M., Callegari, A., Leleu, M., Manley, S., and Suter, D. M. (2016). A role for mitotic bookmarking of sox2 in pluripotency and differentiation. *Genes & development*, 30(22):2538–2550.

Eskicioglu, A. M. and Fisher, P. S. (1995). Image quality measures and their performance. *IEEE Transactions on communications*, 43(12):2959–2965.

Gritti, N., Lim, J. L., Anlaş, K., Pandya, M., Aalderink, G., Martínez-Ara, G., and Trivedi, V. (2021). Morgana: accessible quantitative analysis of organoids with machine learning. *Development*, 148(18):dev199611.

Hama, H., Hioki, H., Namiki, K., Hoshida, T., Kurokawa, H., Ishidate, F., Kaneko, T., Akagi, T., Saito, T., Saido, T., et al. (2015). Sca l es: an optical clearing palette for biological imaging. *Nature neuroscience*, 18(10):1518–1529.

Mulas, C., Kalkan, T., von Meyenn, F., Leitch, H. G., Nichols, J., and Smith, A. (2019). Defined conditions for propagation and manipulation of mouse embryonic stem cells. *Development*, 146(6):dev173146.

Pachitariu, M. and Stringer, C. (2022). Cellpose 2.0: how to train your own model. *Nature methods*, 19(12):1634–1641.

Rhee, J. M., Pirity, M. K., Lackan, C. S., Long, J. Z., Kondoh, G., Takeda, J., and Hadjantonakis, A.-K. (2006). In vivo imaging and differential localization of lipid-modified gfp-variant fusions in embryonic stem cells and mice. *genesis*, 44(4):202–218.

Sánchez-Corrales, Y. E., Hartley, M., Van Rooij, J., Marée, A. F., and Grieneisen, V. A. (2018). Morphometrics of complex cell shapes: lobe contribution elliptic fourier analysis (loco-efa). *Development*, 145(6):dev156778.

Schindelin, J., Arganda-Carreras, I., Frise, E., Kaynig, V., Longair, M., Pietzsch, T., Preibisch, S., Rueden, C., Saalfeld, S., Schmid, B., et al. (2012). Fiji: an open-source platform for biological-image analysis. *Nature methods*, 9(7):676–682.

Serrano Nájera, G. (2021). *Analysis and modulation of cell behaviours driving avian gastrulation.* PhD thesis, School of Life Sciences, University of Dundee.

Serrano Nájera, G., Plum, A. M., Steventon, B., Weijer, C. J., and Serra, M. (2024). Control of modular tissue flows shaping the embryo in avian gastrulation. *bioRxiv*.

Thielicke, W. and Sonntag, R. (2021). Particle image velocimetry for MATLAB: Accuracy and enhanced algorithms in PIVlab. *Journal of Open Research Software*, 9(1):12.

Supplementary movies

- Movie 1 Gastruloid on laminin from day 4 to 5. Scale bar 500 μm.
- Movie 2 Gastruloid on laminin from day 4 to 5 in the presence of CK666 50 μM. Scale bar 500 μm.
- Movie 3 Gastruloids on laminin from day 4 to 5 with CK666 at 25 and 50 μM. Scale bar 500 μm.
- Movie 4 Gastruloid on laminin from day 4 to 5 in the presence of SMIFH2 25 μM. Scale bar 500 μm.

Supplementary Figures

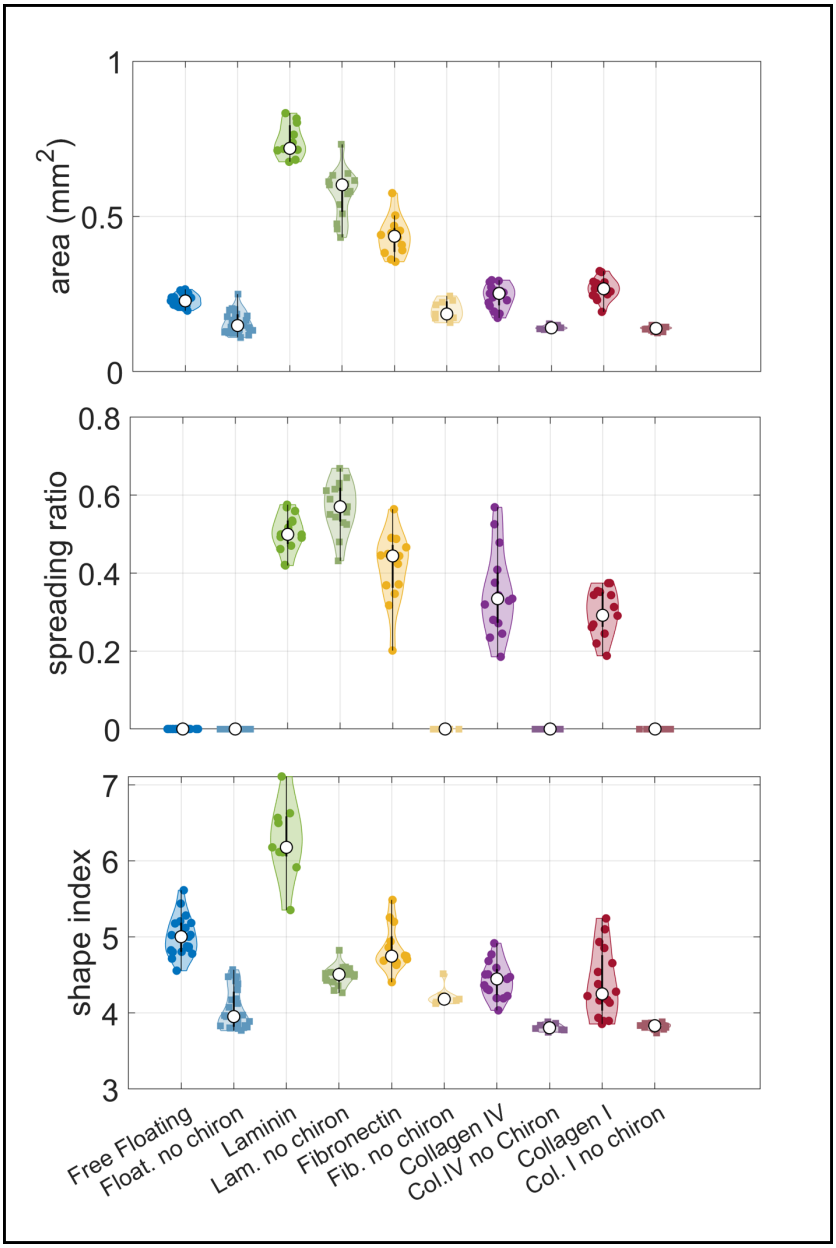

Supplementary Fig. 1. Characterisation of gastruloids grown on different substrates. Analysis of area, migratory abilities (spreading ratio) and elongation (shape index) on day 5 gastruloids grown on different coatings in the presence/absence of Chiron. See the supplementary material for the full statistical analysis.

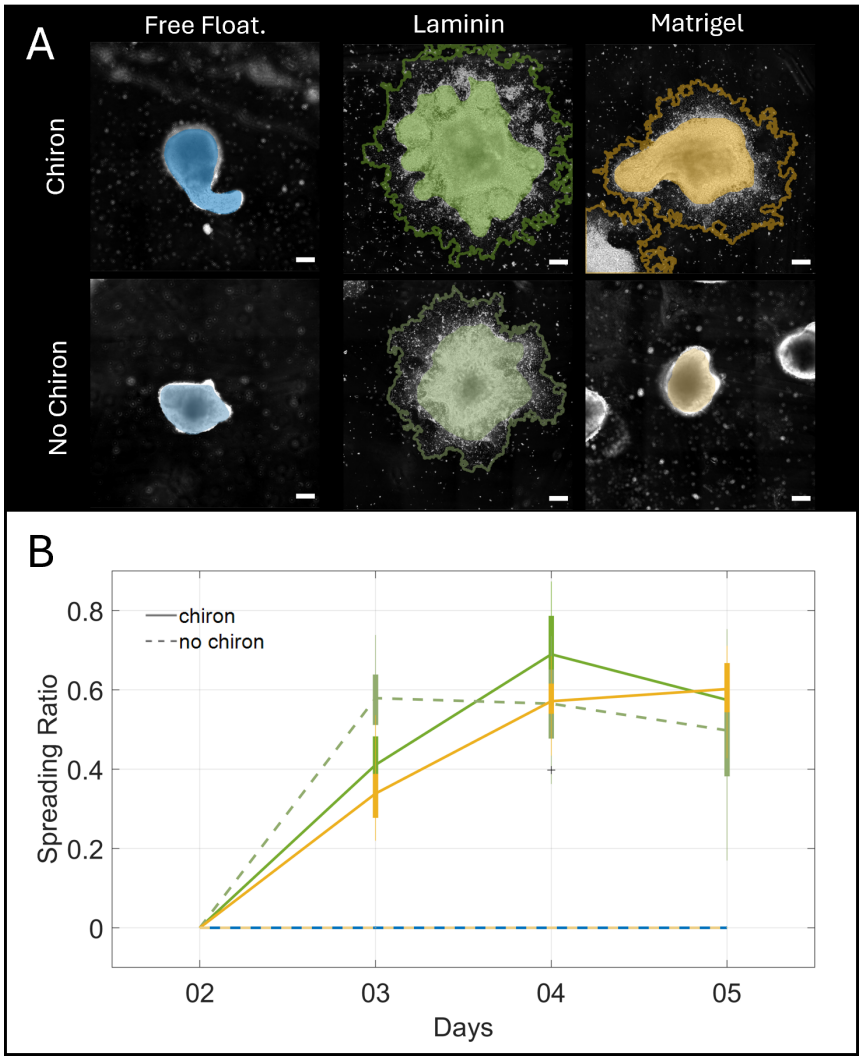

Supplementary Fig. 2. Adhesion to Matrigel requires chiron. A) Representative morphologies depending on the substrate and the presence of chiron. B) Analysis of the spreading capability of gastruloids on different substrates from day 2 to 5. Scale bars $200\mu m$.

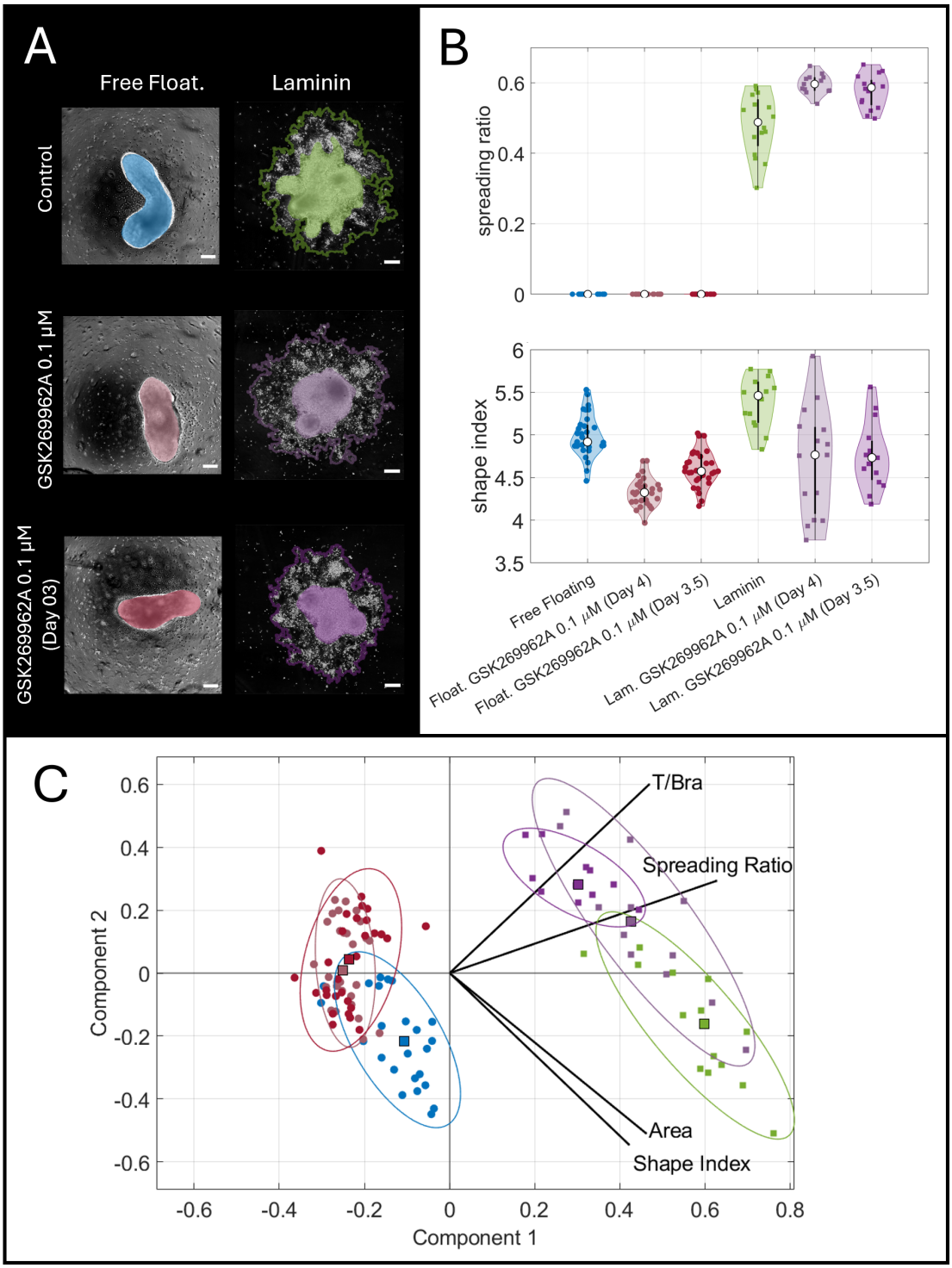

Supplementary Fig. 3. Myosin contractility is necessary for elongation in free-floating and laminin gastruloids. A) Gastruloid morphologies on different substrates with or without the ROCK inhibitor GSK269962A $0.1\mu M$ added on day 3 or 4. B) Top: Analysis of the spreading capabilities after ROCK inhibition. Cell migration is enhanced on laminin. Bottom: Quantification of the shape index after ROCK inhibition. Free-floating and laminin gastruloids show a reduced elongation. C) Principal Component Analysis integrating different properties on day 5. Note that treated free-floating gastruloids do not overlap with the controls. Colours indicate the same conditions across graphs. See the supplementary material for the full statistical analysis.

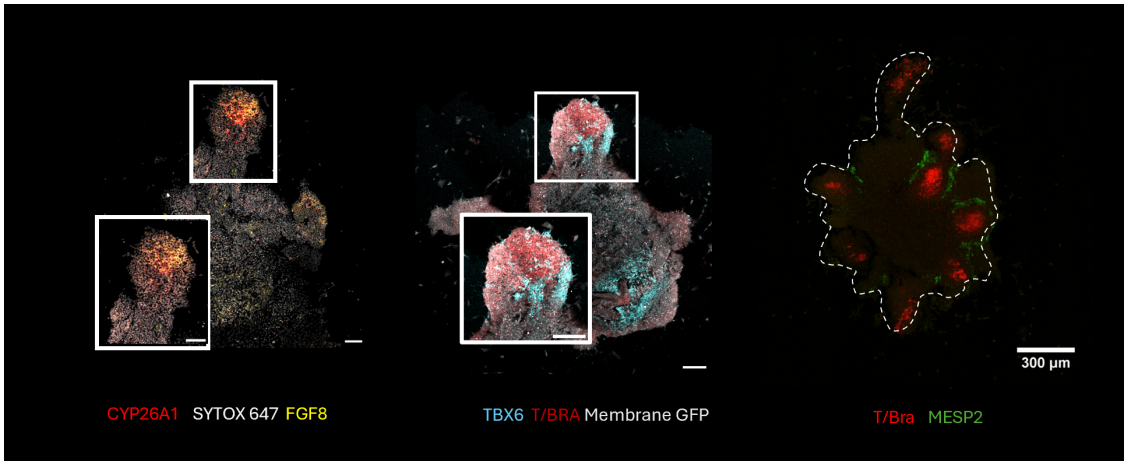

Supplementary Fig. 4. More cell fate markers in gastruloids grown on laminin. A) HCR staining for markers of the posterior tailbud CYP26A1 and FGF8. B) TBX6 (Presomitic mesoderm) and T/Bra (mesoderm). C) MESP2 (Presomitic mesoderm) and T/Bra (mesoderm).

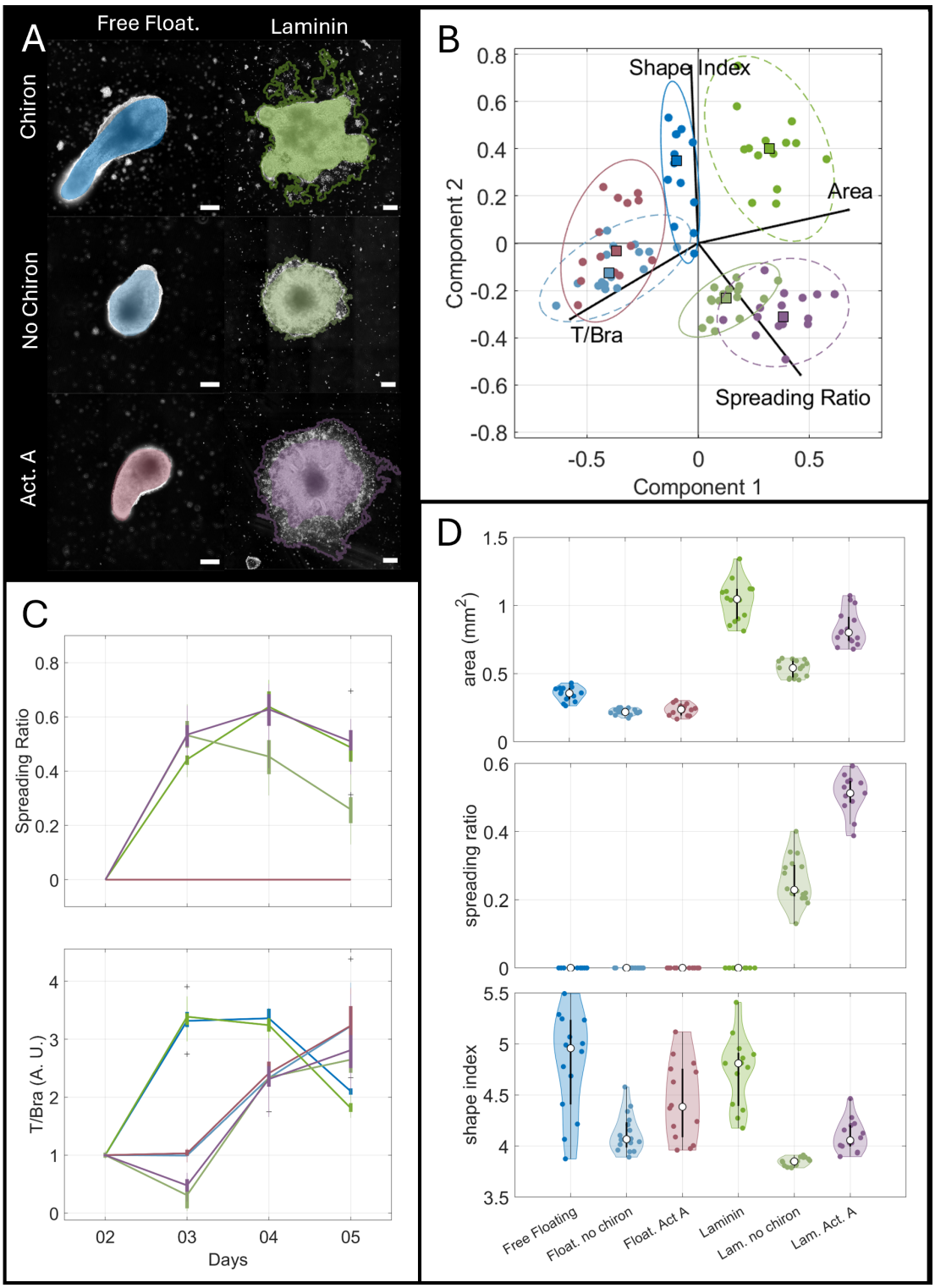

Supplementary Fig. 5. Anterior fates are necessary for cell stream formation. A) Gastruloid morphologies on different substrates with a Chiron pulse or an Activin A pulse on day 2. Only Chiron generates cell streams when seaded on laminin. B) Principal Component Analysis integrating different properties on day 5. C) Analysis of the spreading capability of gastruloids on different substrates (top) and T/Bra expression (bottom) from day 2 to day 5. D) Analysis of area, migratory abilities (spreading ratio) and elongation (shape index) on day 5 gastruloids grown on different coatings in the presence/absence of Chiron. Colours indicate the same conditions across graphs. See the supplementary material for the full statistical analysis.

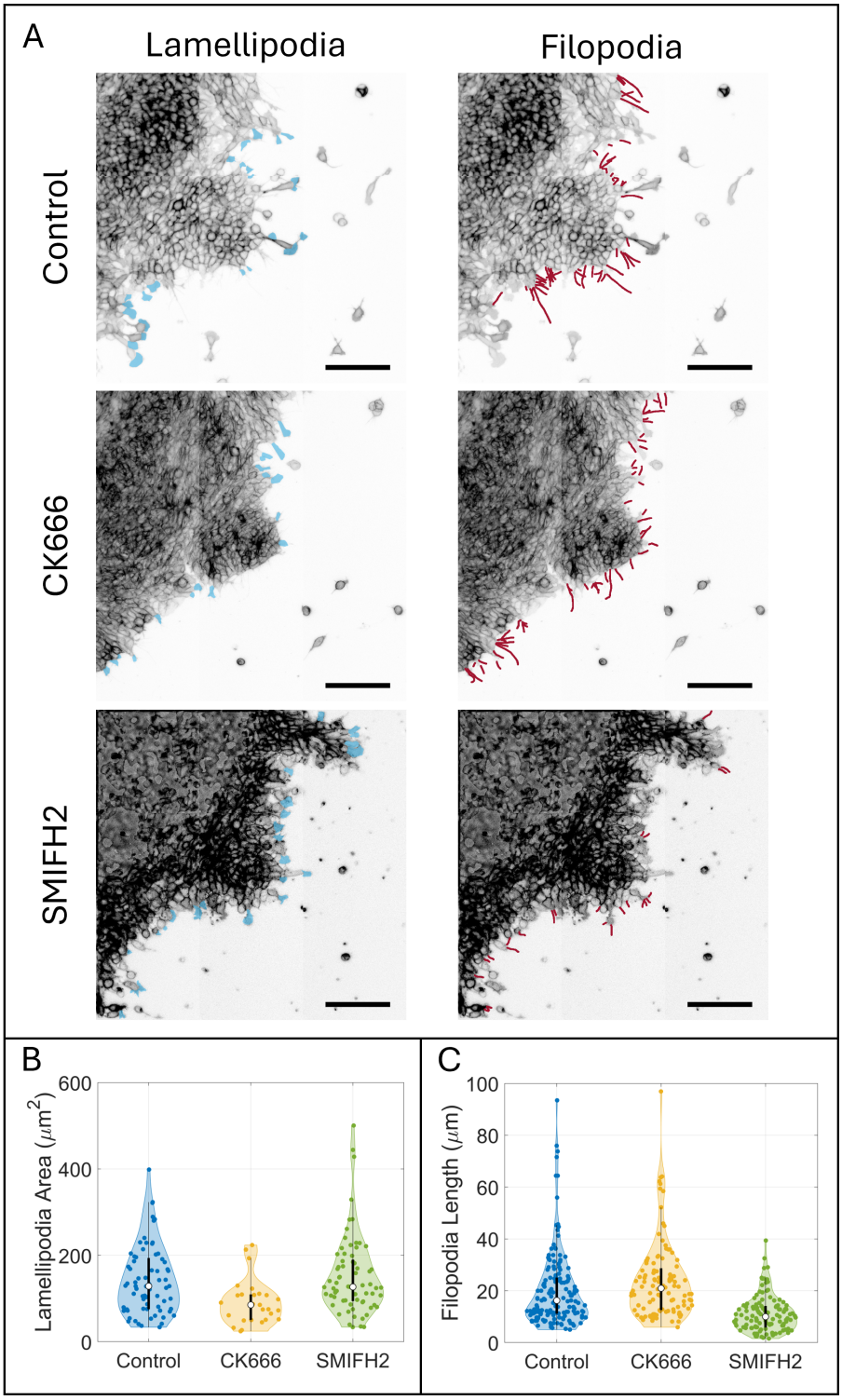

Supplementary Fig. 6. Quantification of Lamellipodia and Filopodia on laminin gastruloids. A) Demonstration of the manual labelling of lamellipodia (left) and filopodia (right) and its morphology with different inhibitors. B) Quantification of lamellipodia area. C) Quantification of filopodia length. See the supplementary material for the full statistical analysis.

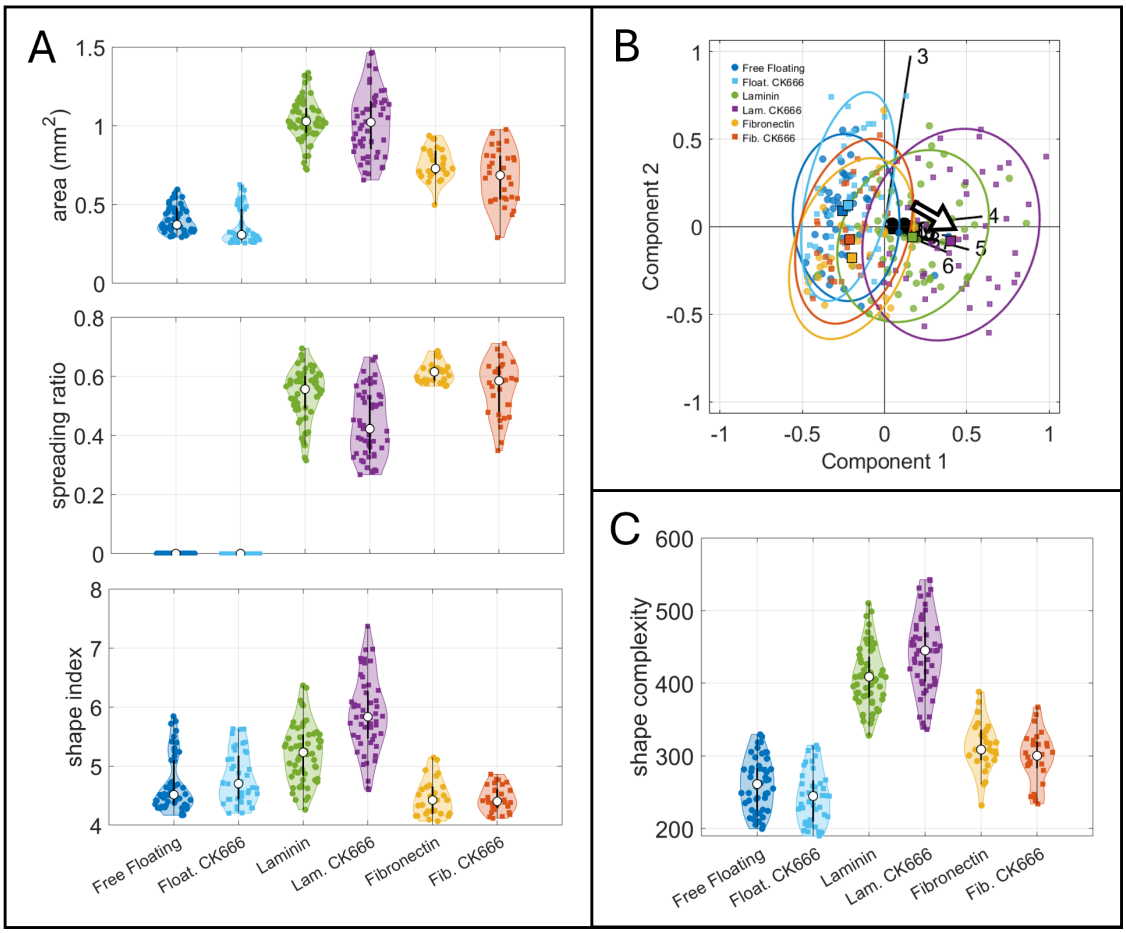

Supplementary Fig. 7. Characterisation of lamellipodia inhibition on different substrate. Analysis of area, migratory abilities (spreading ratio) and elongation (shape index) on day 5 gastruloids grown on different coatings in the presence/absence of CK666 $50\mu M$. B) LOCO-EFA modes for the different morphologies. Arrow indicates the need of higher frequency modes to describe the shapes on laminin gastruloids when in presence of the CK666. C) Shape complexity estimated using of the contribution of LOCO-EFA high frequency modes (see methods). See supplementary material for the full statistical analysis.

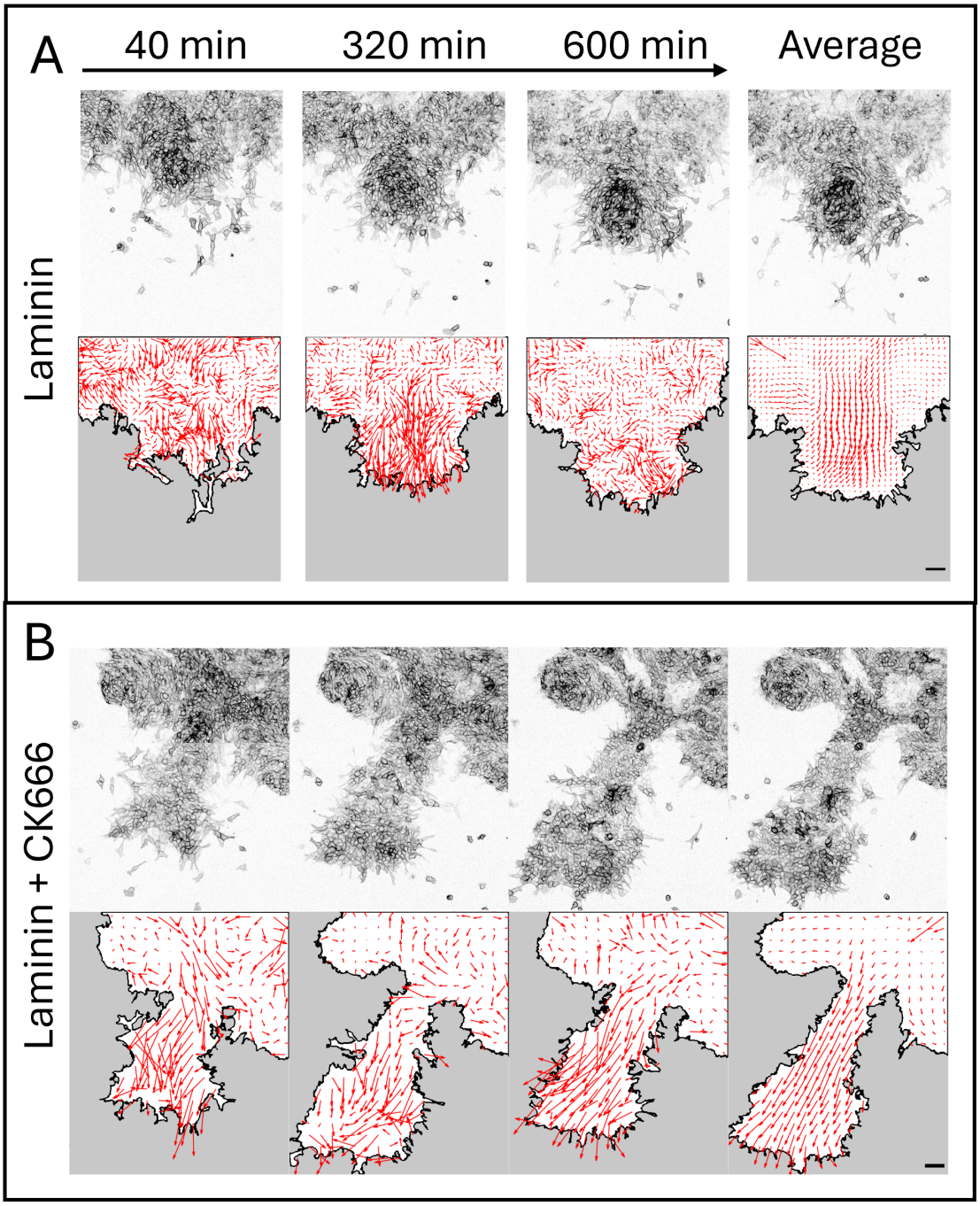

Supplementary Fig. 8. Quantification of tissue flows during cell stream formation. A) Particle Image Velocimetry on laminin and B) in the presence of CK666 $50\mu M$. Scale bars $200\mu m$.

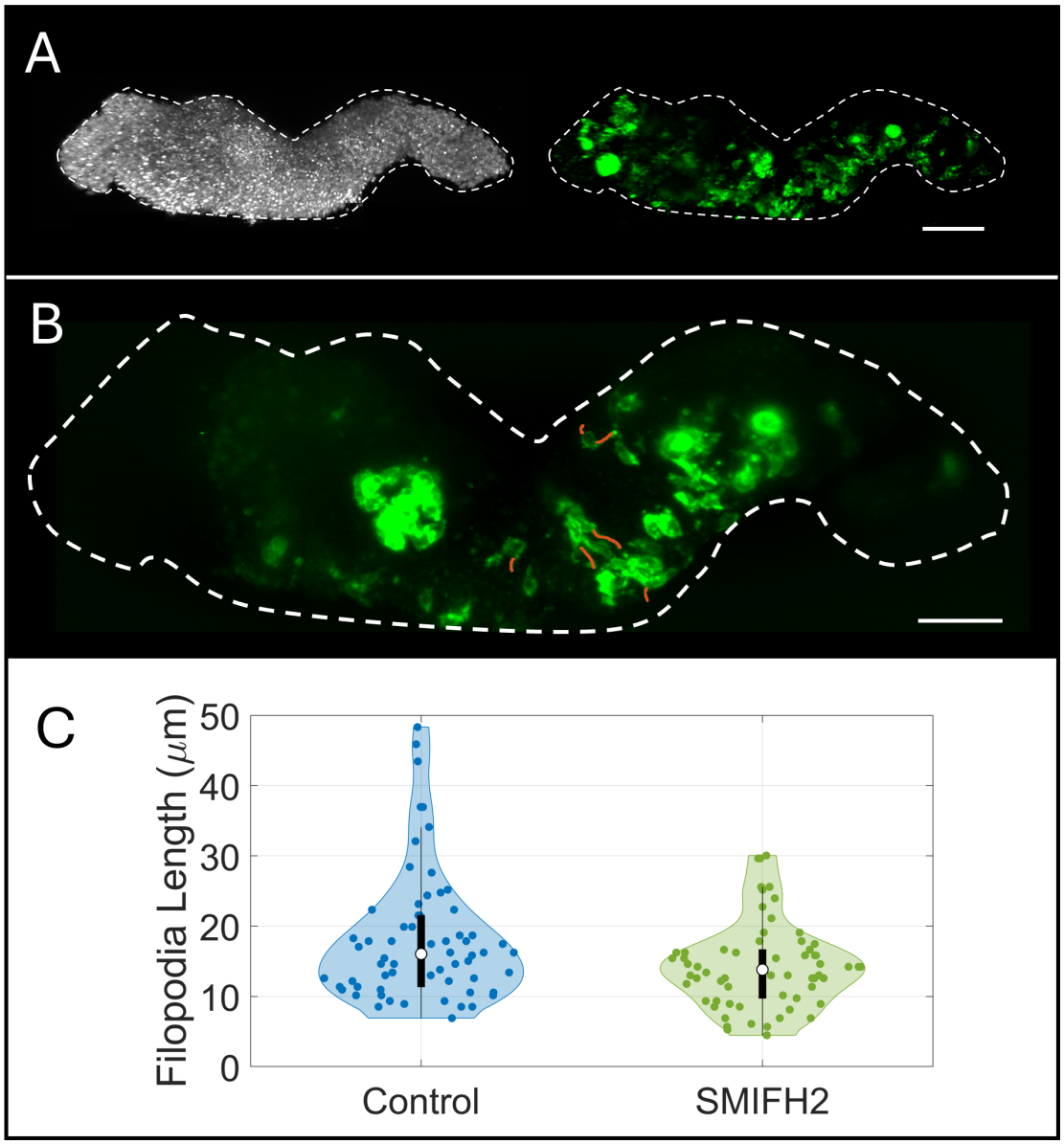

Supplementary Fig. 9. Quantification of Filopodia on free-floating gastruloids. A) Mosaic gastruloid (5% mGFP/ 95% SBN) for quantification of cellular protrusions. B) Demonstration of the manual labelling of filopodia. C) Quantification of filopodia length. See the supplementary material for the full statistical analysis.

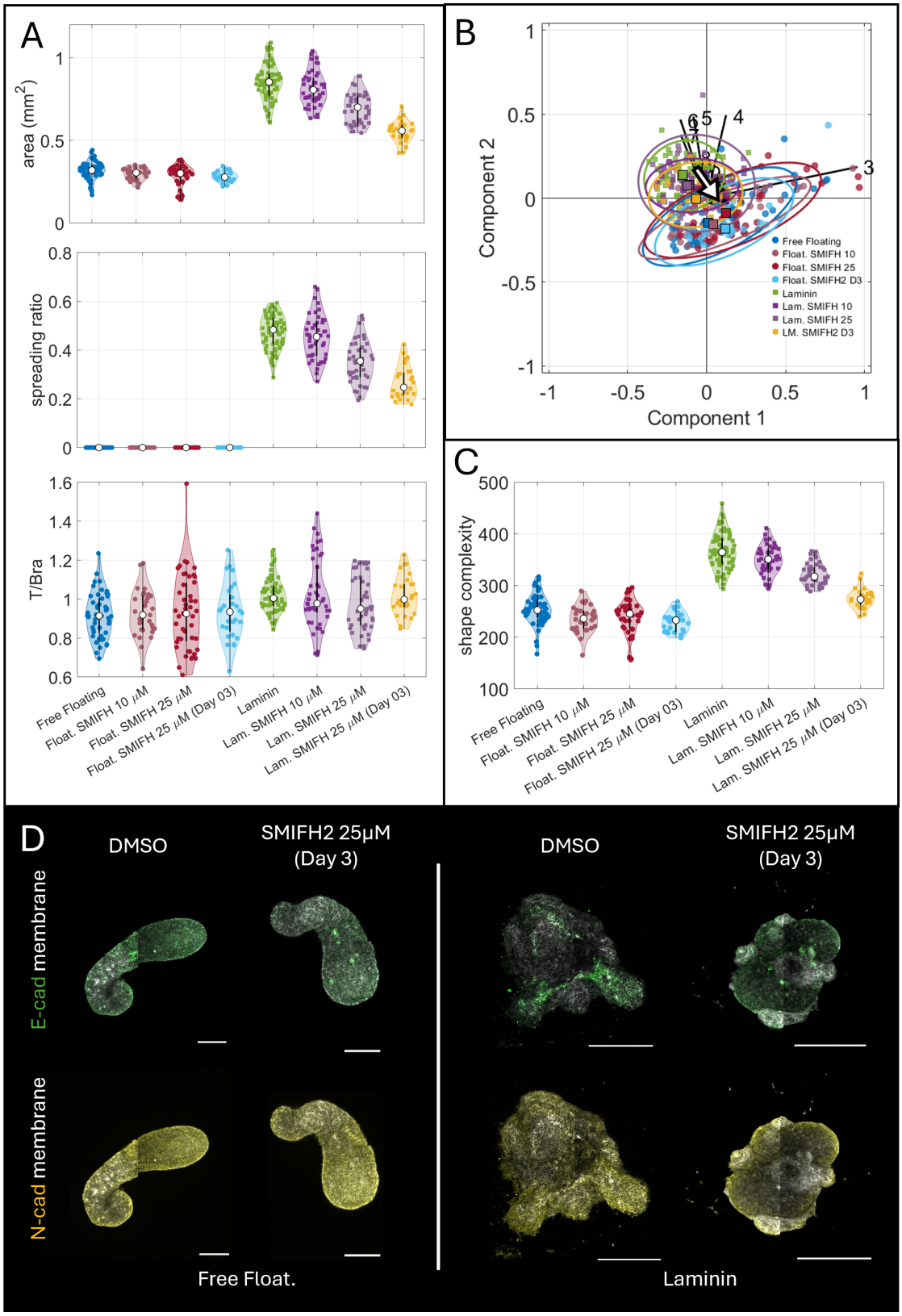

Supplementary Fig. 10. Characterisation of filopodia inhibition on different substrate. Analysis of area, migratory abilities (spreading ratio) and T/Bra expression on day 5 gastruloids, grown free floating or on laminin in the presence/absence of SMIFH2 25μM. B) LOCO-EFA modes for the different morphologies. Arrow indicates the decrease of higher frequency modes to describe the shapes on laminin gastruloids when in presence of the SMIFH2. C) Shape complexity estimated using of the contribution of LOCO-EFA high frequency modes (see methods). D) E-cadh and N-cadh expression on day 5 after in the presence of SMIFH2. See supplementary material for the full statistical analysis.